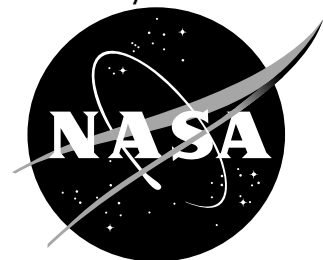NASA/TM-2007-214897

Parametric Study of Flow Control Over a Hump Model Using an Unsteady Reynolds-Averaged Navier-Stokes Code

Christopher L. Rumsey
Langley Research Center, Hampton, Virginia

David Greenblatt
Berlin University of Technology, Berlin, Germany

September 2007

The NASA STI Program Office ... in Profile

Since its founding, NASA has been dedicated to the advancement of aeronautics and space science. The NASA Scientific and Technical Information (STI) Program Office plays a key part in helping NASA maintain this important role.

The NASA STI Program Office is operated by Langley Research Center, the lead center for NASA's scientific and technical information. The NASA STI Program Office provides access to the NASA STI Database, the largest collection of aeronautical and space science STI in the world. The Program Office is also NASA's institutional mechanism for disseminating the results of its research and development activities. These results are published by NASA in the NASA STI Report Series, which includes the following report types:

- TECHNICAL PUBLICATION. Reports of completed research or a major significant phase of research that present the results of NASA programs and include extensive data or theoretical analysis. Includes compilations of significant scientific and technical data and information deemed to be of continuing reference value. NASA counterpart of peer-reviewed formal professional papers, but having less stringent limitations on manuscript length and extent of graphic presentations.

- TECHNICAL MEMORANDUM. Scientific and technical findings that are preliminary or of specialized interest, e.g., quick release reports, working papers, and bibliographies that contain minimal annotation. Does not contain extensive analysis.

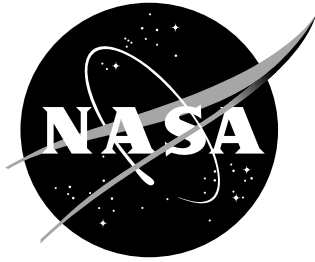- CONTRACTOR REPORT. Scientific and technical findings by NASA-sponsored contractors and grantees.

- CONFERENCE PUBLICATION. Collected papers from scientific and technical conferences, symposia, seminars, or other meetings sponsored or co-sponsored by NASA.

- SPECIAL PUBLICATION. Scientific, technical, or historical information from NASA programs, projects, and missions, often concerned with subjects having substantial public interest.

- TECHNICAL TRANSLATION. English-language translations of foreign scientific and technical material pertinent to NASA's mission.

Specialized services that complement the STI Program Office's diverse offerings include creating custom thesauri, building customized databases, organizing and publishing research results ... even providing videos.

For more information about the NASA STI Program Office, see the following:

- Access the NASA STI Program Home Page at *http://www.sti.nasa.gov*

- E-mail your question via the Internet to help@sti.nasa.gov

- Fax your question to the NASA STI Help Desk at (301) 621-0134

- Phone the NASA STI Help Desk at (301) 621-0390

- Write to:
  NASA STI Help Desk
  NASA Center for AeroSpace Information
  7115 Standard Drive
  Hanover, MD 21076-1320

NASA/TM-2007-214897

Parametric Study of Flow Control Over a Hump Model Using an Unsteady Reynolds-Averaged Navier-Stokes Code

Christopher L. Rumsey
Langley Research Center, Hampton, Virginia

David Greenblatt
Berlin University of Technology, Berlin, Germany

Parametric Study of Flow Control Over a Hump Model Using an Unsteady Reynolds-Averaged Navier-Stokes Code

Christopher L. Rumsey[*]

NASA Langley Research Center, Hampton, VA 23681-2199, USA

David Greenblatt[†]

Berlin University of Technology, Berlin, Germany

This is an expanded version of a limited-length paper that appeared at the 5th International Symposium on Turbulence and Shear Flow Phenomena by the same authors.[1] A computational study was performed for steady and oscillatory flow control over a hump model with flow separation to assess how well the steady and unsteady Reynolds-averaged Navier-Stokes equations predict trends due to Reynolds number, control magnitude, and control frequency. As demonstrated in earlier studies, the hump model case is useful because it clearly demonstrates a failing in all known turbulence models: they under-predict the turbulent shear stress in the separated region and consequently reattachment occurs too far downstream. In spite of this known failing, three different turbulence models were employed to determine if trends can be captured even though absolute levels are not. Overall the three turbulence models showed very similar trends as experiment for steady suction, but only agreed qualitatively with some of the trends for oscillatory control.

I. Introduction

The effective control of flow separation promises substantial performance improvements for a wide variety of air vehicles. Although the methods are well known, there is very little by way of theory or numerical models that can adequately predict lift enhancements, drag reduction, etc. An attempt was made to address this problem by conducting a CFD validation workshop (CFDVAL2004) for synthetic jets and turbulent separation control[2] where one case was dedicated to predicting the nominally two-dimensional flow over a hump. The baseline (uncontrolled) case was considered in addition to control by means of steady suction[3] and zero-net-mass flux (oscillatory) blowing.[4] The workshop determined that CFD with steady or unsteady Reynolds-averaged Navier-Stokes (RANS or URANS) consistently over-predicted the reattachment location, regardless of turbulence model or method. Within the separation bubble, most computations predicted velocity profiles reasonably well but considerably under-predicted the magnitude of turbulent shear stresses. This under-prediction of turbulence within the bubble caused delayed flow reattachment. Large-eddy simulations and other computationally expensive methods appear capable of overcoming this deficiency. See, e.g., Krishnan et al.,[5] Morgan et al.,[6] and Saric et al.[7] The focus of the current study is on the more affordable RANS and URANS methodologies.

Although the individual test cases from CFDVAL2004 were challenging to CFD codes, only single test cases were considered for both steady suction and zero-net-mass flux blowing. In the earlier work of Rumsey,[8] computational results were evaluated against these workshop test cases, with a focus on the zero-net-mass flux blowing case. During the course of the experimental investigation, however, steady and unsteady surface pressures were acquired for a wide variety of control parameters, including Reynolds number, suction flow rate, and frequency and blowing amplitude in the zero-net-mass flux case. By comparing trends of numerical results with experimental data, it should be possible to draw more precise conclusions regarding CFD's value for predictive purposes. Furthermore, a number of important experimental observations were made and it is not known if CFD codes are capable of predicting them. For example, by varying the suction flow rate and comparing these results to high Reynolds number data, the control effectiveness was found to increase substantially with increasing Reynolds number. In addition, for the oscillatory case, the flow was seen to be highly dependent on control frequency and peak blowing amplitude. Different, sometimes counteracting,

---

[*]Senior Research Scientist, Computational Aerosciences Branch, Mail Stop 128, c.l.rumsey@nasa.gov.

[†]Senior Research Scientist, Institute of Fluid Dynamics and Engineering Acoustics, 8 Mueller-Breslau Street, david.greenblatt@pi.tu-berlin.de.

mechanisms dominated the separated flowfield during different parts of the control cycle. To explore some of these issues, a detailed parametric study using the URANS equations is described here.

II. Computational Method

The computer code CFL3D (Krist et al.[9]) solves the three-dimensional, time-dependent, Reynolds-averaged compressible full Navier-Stokes equations with an upwind finite-volume formulation (it is exercised in two-dimensional mode of operation for the 2-D cases in this study). The Navier-Stokes equations are averaged using Favre averaged variables. Upwind-biased spatial differencing is used for the inviscid terms, and viscous terms are centrally differenced. In time-accurate mode, CFL3D uses pseudo-time stepping with multigrid and achieves second order temporal accuracy. With pseudo-time stepping, subiterations are used to reduce the linearization and factorization errors, and advance the solution to the next physical time.

Three different turbulence models are used in the current study: the Spalart-Allmaras (SA) model,[10] Menter's k-omega SST model,[11] and the nonlinear explicit algebraic stress model in k-omega form (EASM-ko).[12] The turbulence models are implemented uncoupled from the mean-flow Navier-Stokes equations. They are solved using an implicit approximate factorization approach (number of factors depends on dimensionality).

III. Results

A. Flowfield Conditions

The wall-mounted hump model had a chord of $c = 0.42$ m, height of 0.0538 m at its maximum thickness point, and width of 0.5842 m. The configuration was two-dimensional, and experimental results were demonstrated to be nominally 2-D by means of stereoscopic PIV, surface pressure measurements, and wall shear stress measurements. The flow control slot was located near 65% c; this was close to where the flow separated in its uncontrolled state. A summary of the flowfield conditions studied is provided in Tables 1 and 2. A star appears next to the particular cases used in the workshop in 2004. The Mach number for all computations was $M = 0.1$. For the steady suction cases, the steady mass transfer momentum coefficient is defined by:

$$c_\mu = \frac{\rho_j h U_j^2}{cq} \tag{1}$$

where $h = 0.00187c$ is the slot height, U_j is the total jet velocity, and q is the freestream dynamic pressure. The c_μ corresponds with a steady mass flow rate (given by $\dot{m}$) sucked through the slot. For the unsteady oscillatory cases, the oscillatory flow momentum coefficient is defined by:

$$\langle c_\mu \rangle = \frac{\rho_j h \langle U_j \rangle^2}{cq} \tag{2}$$

where $\langle U_j \rangle$ is the root-mean-square of the total jet velocity. The c_μ and $\langle c_\mu \rangle$ parameters are typically used in experiments to characterize flow-control blowing levels and are cited as percentages throughout this paper. However, for the purposes of CFD, it is much easier to characterize the levels using $\dot{m}$ for steady suction and by maximum outflow velocity U_{peak} for oscillatory control. Furthermore, for the oscillatory cases, the reduced excitation frequency is defined as $F^+ = fX/U_\infty$, where X is the distance from the slot to flow reattachment point for no flow control. For the purposes of CFD, it is easier to use f. A great deal of additional information concerning this case can be found on the website for the validation workshop. [a]

B. Computational Details

A 2-D fine-level 4-zone grid was created with 208,320 cells. The jet slot and cavity were included in the hump model computations. Many of the computations used a "medium level" version of the grid consisting of every other point in each coordinate direction, or 52,080 cells. Several grid studies were performed, both here as well as in previous work for the workshop cases.[8] These studies indicated that there were only very small differences between mean flow quantities (either long-time-averaged or phase-averaged) on the two grid levels for the 2004 workshop conditions, and less than 5% difference in turbulence quantities. Time step studies were also performed for the oscillatory control case,

---

[a]http://cfdval2004.larc.nasa.gov, [cited 3/2007].

Table 1. Steady suction cases.

$Re \times 10^6$	c_μ, %	$\dot{m}$, kg/s
0.5574	0.24	0.0152
0.5574	0.73	0.0263
0.5574	2.59	0.0495
0.936	0.030	0.0053
0.936	0.076	0.0084
*0.936	0.24	0.0152
0.936	0.47	0.0208
0.936	0.73	0.0263
2.0	0.03	0.0053
2.0	0.24	0.0152
2.0	0.47	0.0208
16.0	0.03	0.0053
16.0	0.24	0.0152
16.0	0.47	0.0208
32.0	0.03	0.0053
32.0	0.24	0.0152

and indicated that using at least 180 steps per period in conjunction with 20 subiterations per time step was sufficient to yield little perceptible change in results. For all results to be shown here, 360 steps per period were used.

Two different grid families were used, depending on the Reynolds number. Both had the same number of points, but the grid used for $Re = 16$ and 32 million had a finer minimum spacing at the wall, $\Delta y/c = 1 \times 10^{-6}$ on the finest level (compared with $\Delta y/c = 8 \times 10^{-6}$ for the grid used at lower Re). On the medium level, this spacing yielded an average minimum y^+ of 1.5 at $Re = 32$ million, and 0.8 at 16 million, where y^+ represents normal-distance wall units $y\sqrt{(\tau_w/\rho)}/\nu$. At the various lower Re employed, the average minimum y^+ was at most 1.1 on the medium level. All grids extended from $x/c = -6.39$ upstream to 4.0 downstream. The top tunnel wall was included, although the shape was slightly altered to account for blockage caused by the endplates.[8] A view of the medium level grid (52,080 cells) used for Re of 2 million or less is shown in Fig. 1, and a view of both grids near the region of the slot is shown Fig. 2.

The boundary conditions were as follows. At the floor and hump surfaces, as well as at the side walls inside the cavity, solid wall adiabatic boundary conditions were applied. At the front of the grid, a far-field Riemann-type boundary condition was applied. At the downstream boundary the pressure was set to approximately freestream, and all other quantities were extrapolated from the interior of the domain. The top tunnel wall was treated as an inviscid wall for all of the computations shown here. At the bottom of the cavity, the boundary condition for steady suction set the u-velocity component to 0 and v-velocity such that the mass flow matched experiment. For the oscillatory cases the velocity components were set with $u = 0$ and $v = [(\rho v)_{\max}/\rho]cos(2\pi ft)$, where f is the frequency and t is the time, and $(\rho v)_{\max}$ was chosen in order to achieve a maximum outflow velocity magnitude at the exit plane near to the target U_{peak} from the experiment.

C. Results for Steady Suction

As mentioned in the Introduction, historically all RANS methods applied to this case have yielded results with too long a separation bubble, because they under-predicted the magnitude of the turbulent shear stress in the separated region. An example is shown in Fig. 3. Here, experimental streamlines for the steady suction case from the workshop are compared with CFD results using the three turbulence models SA, SST, and EASM-ko. In the experiment, the flow reattached near $x/c = 0.94$, but in the CFD, the reattachment occurred at $x/c = 1.10$ for SA, 1.13 for SST, and 1.16 for EASM-ko.

For the current study, the effect of grid density on surface pressures for different c_μ is shown in Fig. 4 for the SA model. There were almost no differences in results using the two different grids at the lowest blowing coefficient levels,

Table 2. Unsteady oscillatory control cases.

$Re \times 10^6$	$\langle c_\mu \rangle$, %	U_{peak}, m/s	F^+	f, Hz
0.936	0.11	27	0.46	83.1
0.936	0.013	8	0.77	138.5
*0.936	0.11	27	0.77	138.5
0.936	0.354	48	0.77	138.5
0.936	0.11	27	1.39	249.3
0.936	0.11	27	2.00	360.1
16.0	0.11	27	0.77	138.5

and relatively small differences at the higher levels. For example, at the highest blowing coefficient of $c_\mu = 0.76$, the fine grid bubble was longer than the medium grid bubble by about 7%.

Results using the three turbulence models tested are given in Fig. 5 for all five of the steady suction levels at $Re = 0.936$ million. In every case, the SA model gave the best agreement with experiment and EASM-ko the worst, but all three models were reasonably similar to each other. The computed pressures in the region between $x/c = 0.65$ and 1.2 were all quite different from experiment. At the higher blowing coefficients, the differences between the turbulence models were smaller than the differences between CFD and experiment.

In spite of the fact that we know that CFD using RANS is incapable of obtaining the same quantitative result as experiment in terms of reattachment position, we turn to the question of whether it is capable of predicting trends. Fig. 6 gives surface pressure coefficients at $Re = 0.936$ million for a range of different c_μ coefficients (0.030%, 0.076%, 0.24%, 0.47%, and 0.73%). Using the SA model, the CFD exhibited a similar trend as experiment, but the physical details were clearly not correctly modeled. As c_μ increased, the separation extent decreased similarly for CFD and experiment, but the CFD predicted a pressure drop downstream of the slot instead of a steeper pressure recovery observed in the experiment. The c_p levels over the forward portion of the hump agreed extremely well with experiment at all c_μ conditions. Fig. 7 shows the same type of plot for the other two turbulence models. Here, the agreement with experiment was worse than the agreement using SA, but the general trend of decreasing separation with increasing c_μ was similar. The c_p levels over the forward portion of the hump were not in as good agreement with experiment as seen with the SA model.

A different way of looking at the data is shown in Fig. 8 for the SA model. Here, Δc_p is plotted, showing the change in surface pressure coefficient of the controlled flow relative to baseline (no control). Both CFD and experiment predicted increasing pressures in the bubble relative to baseline as c_μ was increased, but CFD yielded smaller Δc_p levels and its peaks were further downstream. The smaller levels indicate that the CFD predicted smaller influence than experiment for any given level of suction applied (relative to baseline). The peaks were further downstream because CFD predicted a longer bubble than experiment. Fig. 9 shows the same type of plot for the other two turbulence models. As before, the absolute agreement between SST or EASM-ko with experiment was worse, but the trends were similar. The predicted levels were very close between the three models (with EASM-ko only slightly higher than the others), but SST and EASM-ko predicted longer bubbles, so the peaks in the Δc_p curves were further downstream.

In the experiment, Greenblatt et al.[3] noted a clear Reynolds number effect both at $c_\mu = 0.24$ and $c_\mu = 0.47$, despite the small Reynolds number range tested (from $Re = 0.557$ million to 1.1 million). Comparisons with a similar hump model[13] at a much higher Reynolds number of 16 million showed a continuing Reynolds number effect, which was most evident when comparing form-drag on the respective models (see discussion below). In the CFD results, there was also a clear trend of increasing effectiveness with increasing Reynolds number, as shown in Fig. 10 for the SA model on the fine grid. The largest differences occurred below a Re of 16 million. Similar results are shown in Fig. 11 for all three models on the medium grid (only two different Reynolds numbers were tested for the SST and EASM-ko models). The trend with Reynolds number is similar.

This trend is further elucidated in Fig. 12, which summarizes the effect of c_μ and Re on bubble length (X_B/c) for the SA model on the fine grid. Here, the general trend of decreasing bubble length with increasing c_μ is evident. The only experimental data available were at the lowest Re of 557,400 and 936,000. The experimental results appeared roughly linear on this log plot. The CFD results were also fairly linear at the lower c_μ, but they tended to drop down at the higher c_μ. Overall, CFD produced a slightly shallower slope than experiment, along with a significantly longer

bubble at the same Re. The change between Re of 557,400 and 936,000 was similar for CFD as experiment. The most dramatic shortening of the bubble, as predicted by the CFD, occurred below $Re = 16$ million; the shortening was small between $Re = 16$ million and 32 million. Coincidentally, the X_B levels from CFD at the highest Re matched fairly well with the experimental levels at the lowest Re.

Fig. 13 shows a plot of the same quantity for all three turbulence models on the medium grid, for two different Reynolds numbers. The experimental results at $Re = 936,000$ are also shown for reference. In this figure, the solid lines represent CFD results at $Re = 936,000$ and the dashed lines $Re = 16$ million. The results for SA are the square symbols, for SST the triangles, and for EASM-ko the inverted the inverted triangles. Here, the trend of longer bubble lengths for the SST and EASM-ko models compared with SA is evident.

Fig. 14 shows the effect of c_μ on pressure drag coefficient. Here, experimental results from Seifert and Pack[13] at a higher Reynolds number of 16 million are also shown. It should be noted, however, that there were geometric differences in the slot region of this earlier experiment that may have resulted in different baseline c_{dp} levels. As noted in Greenblatt et al.,[3] in spite of these differences, overall there was a clear trend of increasing control effectiveness with increasing Re. A similar trend was also evident in the CFD results using SA on the fine grid, although the c_{dp} levels were lower than in the experiments. Fig. 15 shows a plot of the same quantity for all three turbulence models on the medium grid, for two different Reynolds numbers. The SST model consistently yielded the highest c_{dp} levels and SA the lowest. The experimental results at $Re = 936,000$ are also shown for reference.

To better compare the trends, suction results are shown relative to results with no control for $Re = 0.936$ million in Fig. 16. Here, the computed c_{dp} trend relative to baseline for all three turbulence models is in good agreement with experiment relative to its baseline, and computed bubble length trend relative to baseline is of correct magnitude but shallower slope than experiment. This figure indicates that, given a known baseline performance, the RANS tools using the current turbulence models can predict integral trends for suction reasonably well.

D.   Results for Oscillatory Control

Average streamlines for the oscillatory workshop case are shown in Fig. 17 for the three turbulence models compared with experiment. Again, the long-time-averaged bubble size was always over-predicted using RANS. (In the experiment, the mean flow reattached near $x/c = 0.99$, but in the CFD, the mean reattachment occurred at $x/c = 1.22$ for SA, 1.19 for SST, and 1.19 for EASM-ko.) However, as discussed in Rumsey,[8] the relative motion of the large-scale convected vortical flow structures caused by the pulsed jet/suction were predicted fairly well compared with experiment for the workshop case. Figs. 18 - 21 show comparisons of phase-averaged c_p at four different phases in the cycle for different $\langle c_\mu \rangle$ and different F^+. Similar to for the workshop case, overall the three turbulence models gave results in reasonable qualitative agreement with experiment for all conditions. However, EASM-ko tended to maintain stronger vortices and yield larger peaks in pressure (particularly for $F^+ = 0.46$). All of the oscillatory computations used the medium grid. As mentioned earlier, grid and time step studies for the oscillatory control case were performed in Rumsey.[8]

Figs. 22 - 25 show color vorticity contours for the workshop conditions of $F^+ = 0.77$, $\langle c_\mu \rangle = 0.11\%$ at four times during the cycle. During each cycle, a vortex forms and convects downstream. The SA model diffused the shed vortex the most, in generally good agreement with experiment, whereas both SST and EASM-ko preserved the vortex strength farther downstream. All three models predicted reasonably well the general position of the vortex immediately after it had been shed, but the vortex in the experiment appeared to convect more rapidly than the computations when it was located past $x/c \approx 1.1$.

Additional color vorticity contours for different oscillatory conditions are shown next. However, because PIV data were only taken at the workshop conditions, experimental results were not available for comparison. Figs. 26 - 29 show computed results at the lower blowing condition of $\langle c_\mu \rangle = 0.013\%$. The main differences between these results and those at the workshop conditions are that the vortices are weaker in strength, and they convect somewhat further for the same time in the cycle. Figs. 30 - 33 show computed results at the higher blowing condition of $\langle c_\mu \rangle = 0.354\%$. At this condition, the individual vortices appear to form or split away from the wall region earlier. After convecting downstream, the SST and EASM-ko results indicate more rapid diffusion of the vortical structures than for results using the same models at the workshop conditions, whereas SA results indicate the opposite. Figs. 34 - 37 show computed results at the same blowing strength as the workshop conditions, but at the lower frequency of $F^+ = 0.46$. Figs. 38 - 41 are at the higher frequency of $F^+ = 2.00$. At the lower frequency, the vortical blobs of fluid tend to be larger in size, and exhibit a larger range of motion and extent. At the higher frequency, the vortices are tighter and are constrained to travel within a narrower band.

The effect of Reynolds number on long-time-averaged c_p is shown in Fig. 42 for the SA model. Here, the experimental results at $Re = 16$ million are from Seifert and Pack,[13] so small geometric and setup differences may have

caused some of the differences in experimental results. Between $Re = 0.936$ million and 16 million, CFD exhibited a small increase of control effectiveness: the bubble length decreased from $X_B/c = 0.601$ to 0.536 and c_{dp} decreased slightly from 0.023 to 0.022. Results using SST and EASM-ko, shown in Fig. 43, were qualitatively similar to SA. Compared to the steady suction results of Fig. 10, the computed oscillatory results indicate a much weaker Reynolds number effect between $Re = 0.936$ million and 16 million. This finding appears to be consistent with the results of Greenblatt et al.,[3,4] who noted a definite Reynolds number influence over a limited Reynolds number range (0.58 million to 1.1 million) for steady suction, but no influence for oscillatory blowing, possibly due to saturation of control authority.

The effect of $\langle c_\mu \rangle$ on c_p is shown in Fig. 44, using the SA model. The experiment showed a lowering of the pressure downstream of the slot, accompanied by a shortening of the bubble with increasing $\langle c_\mu \rangle$, but the CFD exhibited almost no difference at all at the two lowest blowing conditions tested. Because of this, a higher blowing velocity not corresponding with any experiment was run ($U_{peak} = 63$ m/s) in order to better establish the trend in the CFD. (This condition is not listed in Table 2 because the precise oscillatory momentum coefficient corresponding to $U_{peak} = 63$ m/s is not known; however, it is estimated to be near $\langle c_\mu \rangle \approx 0.65\%$.) With this additional run included, it is clear that CFD followed a similar trend as experiment at the higher blowing coefficients. The experiment also indicated that the flowfield "saturated" in terms of giving its most negative minimum c_p in the separated region when $\langle c_\mu \rangle = 0.11\%$. In the CFD, there was also a pressure drop in the bubble, but it was more gradual than the experiment and minimum c_p occurred for both $\langle c_\mu \rangle = 0.013\%$ and 0.11%. Then higher $\langle c_\mu \rangle$ produced higher pressure levels in the bubble. Results using SST and EASM-ko, shown in Fig. 45, indicated more of an effect due to $\langle c_\mu \rangle$ at the lowest blowing conditions, but other than this, the trends were similar. The SST and EASM models were not run at the higher $U_{peak} = 63$ m/s condition.

Figs. 46 and 47 show Δc_p, the change in surface pressure coefficient of the controlled flow relative to baseline (no control). In this case, the SST and EASM-ko models yielded better qualitative results than SA compared to experiment, although the peak levels at the highest two $\langle c_\mu \rangle$ values were underpredicted. For SA, only the artificially high $U_{peak} = 63$ m/s began to yield significant positive Δc_p peak levels. Furthermore, at the lowest two control conditions the Δc_p remained negative throughout the "bubble" region for SA, contrary to experiment.

The effect of F^+ on c_p is shown in Fig. 48. In the experiment, increasing F^+ produced slightly smaller separation bubbles up to F^+ near 1.39, but then the trend reversed at higher F^+. In the CFD, no such trend was seen. Instead, if anything, the bubble lengths increased slightly with increasing F^+, but the differences were generally very small. Another noticeable trend in the CFD was a pronounced peak in the minimum bubble pressure at $F^+ = 0.46$, and flatter levels at higher F^+. This peak was even more pronounced for the SST and EASM-ko results, as seen in Fig. 49.

Fig. 50 shows c_{dp} as a function of $\langle c_\mu \rangle$ for two different F^+ using all three turbulence models. As with the steady suction case, the CFD under-predicted the absolute c_{dp} levels, but the general trend of relatively flat c_{dp} for $\langle c_\mu \rangle < 0.11\%$ appears to be similar to experiment. (Compare this plot with Fig. 14, which indicates a negative slope over all of the c_μ range.) In the experiment, this apparent ineffectiveness at low $\langle c_\mu \rangle$ was due to offsetting effects of shortening bubble and increasing pressure drop immediately downstream of the slot, but in the CFD the trend was due to the fact that $\langle c_\mu \rangle$ had little effect on the average pressure distribution. At higher F^+, the CFD predicted lower c_{dp} (like experiment), but the difference was nearly half that seen in the experiment. The three turbulence models differed by as much as 17%, with SST predicting the highest drag levels and SA the lowest. Plotting c_{dp} relative to baseline (Fig. 51) brings CFD results closer to experiment, but levels are still off by as much as $0.005 - 0.007$. Therefore, the statement made in the last section for steady suction cases – that RANS can predict integral trends reasonably well given a known baseline performance – cannot be confidently asserted for the oscillatory cases.

IV. Summary and Conclusions

An extensive computational study was conducted with RANS and URANS and three different turbulence models in application to the hump model case from a flow control validation workshop held in 2004. This paper is an expanded version of a limited-length paper that summarized results from the study and appeared at the 5th International Symposium on Turbulence and Shear Flow Phenomena by the same authors.[1] The current paper contains additional plotted results that could not be shown in the shorter version. Many of the cases from this study were not part of the workshop itself, but were included in the experiment. They included investigations into the effects of Reynolds number, control magnitude, and control frequency. The purpose of this study was to investigate the effectiveness of RANS and URANS CFD for predicting trends in this type of flow control application.

In summary, all three turbulence models performed similarly, in the sense that differences between the models were generally less than differences between CFD and experiment. However, the SA model was usually superior to

the others. For steady suction, CFD appeared capable of predicting the trends due to Reynolds number and c_μ, and this was clearly evident by comparing bubble length and form-drag changes. Nevertheless, absolute levels, such as the pressure recovery details, were not correctly predicted. The fact that both experiment and CFD showed a strong Re effect is important because the majority of experiments are performed at low Reynolds number laboratory conditions ($Re \leq 1,000,000$) and are assumed to remain valid under typical flight conditions with Re at several tens of millions.

For oscillatory control, the CFD indicated increasing effectiveness in the mean with increasing Re, but the effect was not nearly as pronounced as with steady suction. This was consistent with the data of Greenblatt et al.[3,4] When comparing with data of Seifert and Pack,[13] trends due to increasing Re were only crudely captured in the sense that mean bubble length decreased between $Re = 0.936$ million and 16 million, but it was difficult to draw firm conclusions because of slot geometry differences. CFD did not appear to mimic the mean effect of increasing oscillatory momentum coefficient very well. In particular, at levels less than about $\langle c_\mu \rangle = 0.35$, CFD results showed little improvement over no flow control at all. At $\langle c_\mu \rangle > 0.35$, CFD started to show pronounced influence due to higher amplitude blowing/suction. Some effects due to changes in control frequency were captured qualitatively by CFD in the phase-averaged results, but trends in the mean were missed.

References

[1]Rumsey, C. and Greenblatt, D., "Flow Control Predictions Using URANS Modeling: A Parametric Study," 5th International Symposium on Turbulence and Shear Flow Phenomena, TU Munich, Germany, August 27-29, 2007.

[2]Rumsey, C., Gatski, T., Sellers, W., Vatsa, V., and Viken, S., 2006a, "Summary of the 2004 Computational Fluid Dynamics Validation Workshop on Synthetic Jets," *AIAA Journal*, Vol. 44, No. 2, pp. 194–207.

[3]Greenblatt, D., Paschal, K. B., Yao, C.-S., Harris, J., Schaeffler, N. W., and Washburn, A. E., 2006, "Experimental Investigation of Separation Control Part 1: Baseline and Steady Suction," *AIAA Journal*, Vol. 44, No. 12, pp. 2820–2830.

[4]Greenblatt, D., Paschal, K. B., Yao, C.-S., and Harris, J., 2006, "Experimental Investigation of Separation Control Part 2: Zero Mass-Efflux Oscillatory Blowing," *AIAA Journal*, Vol. 44, No. 12, pp. 2831–2845.

[5]Krishnan, V., Squires, K. D., Forsythe, J. R., 2006, "Prediction of Separated Flow Characteristics over a Hump," *AIAA Journal*, Vol. 44, No. 2, pp. 252–262.

[6]Morgan, P. E., Rizzetta, D. P., Visbal, M. R., 2006, "High-Order Numerical Simulation of Turbulent Flow over a Wall-Mounted Hump," *AIAA Journal*, Vol. 44, No. 2, pp. 239–251.

[7]Saric, S., Jakirlic, S., Djugum, A., Tropea, C., 2006, "Computational Analysis of a Locally Forced Flow over a Wall-Mounted Hump at High-Re Number," *Int. Journal of Heat and Fluid Flow*, Vol. 27, No. 4, pp. 707–720.

[8]Rumsey, C., 2007, "Reynolds-Averaged Navier-Stokes Analysis of Zero Efflux Flow Control over a Hump Model," *Journal of Aircraft*, Vol. 44, No. 2, pp. 444–452.

[9]Krist, S. L., Biedron, R. T., and Rumsey, C. L., 1998, "CFL3D User's Manual (Version 5.0)," NASA TM-1998-208444.

[10]Spalart, P. R., and Allmaras, S. R., 1994, "A One-Equation Turbulence Model for Aerodynamic Flows," *La Recherche Aerospatiale*, No. 1, pp. 5–21; also AIAA Paper 92-0439, 1992.

[11]Menter, F. R., 1994, "Two-Equation Eddy-Viscosity Turbulence Models for Engineering Applications," *AIAA Journal*, Vol. 32, No. 8, pp. 1598–1605.

[12]Rumsey, C. L. and Gatski, T. B., 2003, "Summary of EASM Turbulence Models in CFL3D with Validation Test Cases," NASA/TM-2003-212431.

[13]Seifert, A., and Pack, L. G., 2002, "Active Flow Separation Control on Wall-Mounted Hump at High Reynolds Numbers," *AIAA Journal*, Vol. 40, No. 7, pp. 1363–1372.
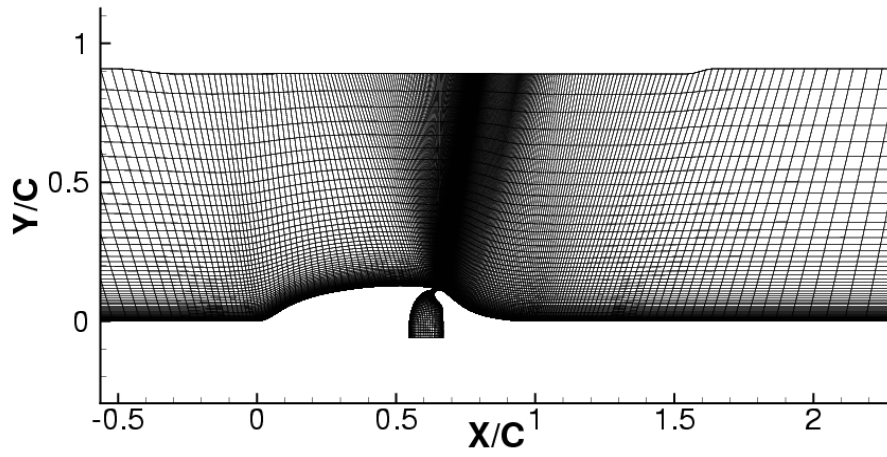
Figure 1. View of medium-level grid (52,080 cells).
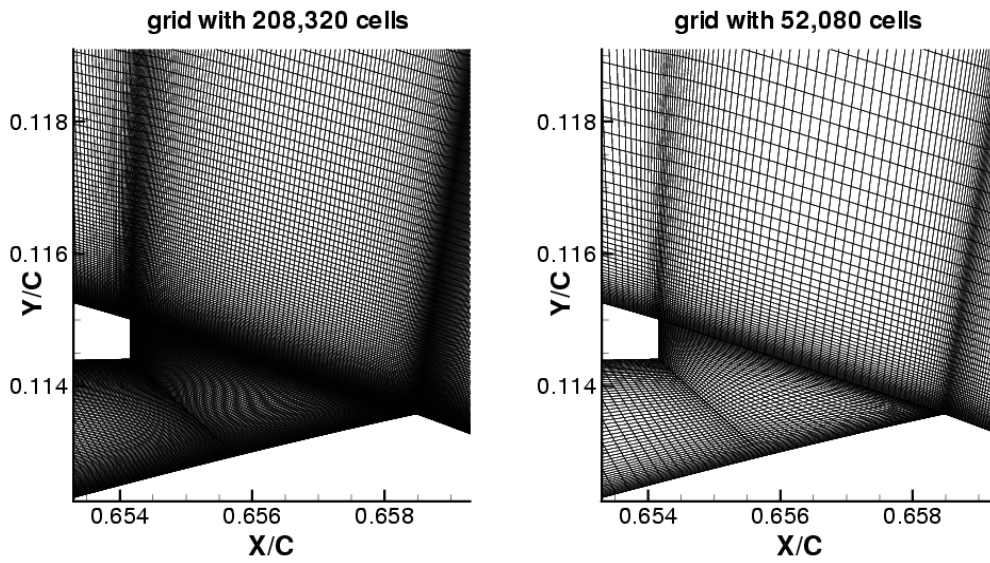
Figure 2. View of both fine and medium grids near slot region.
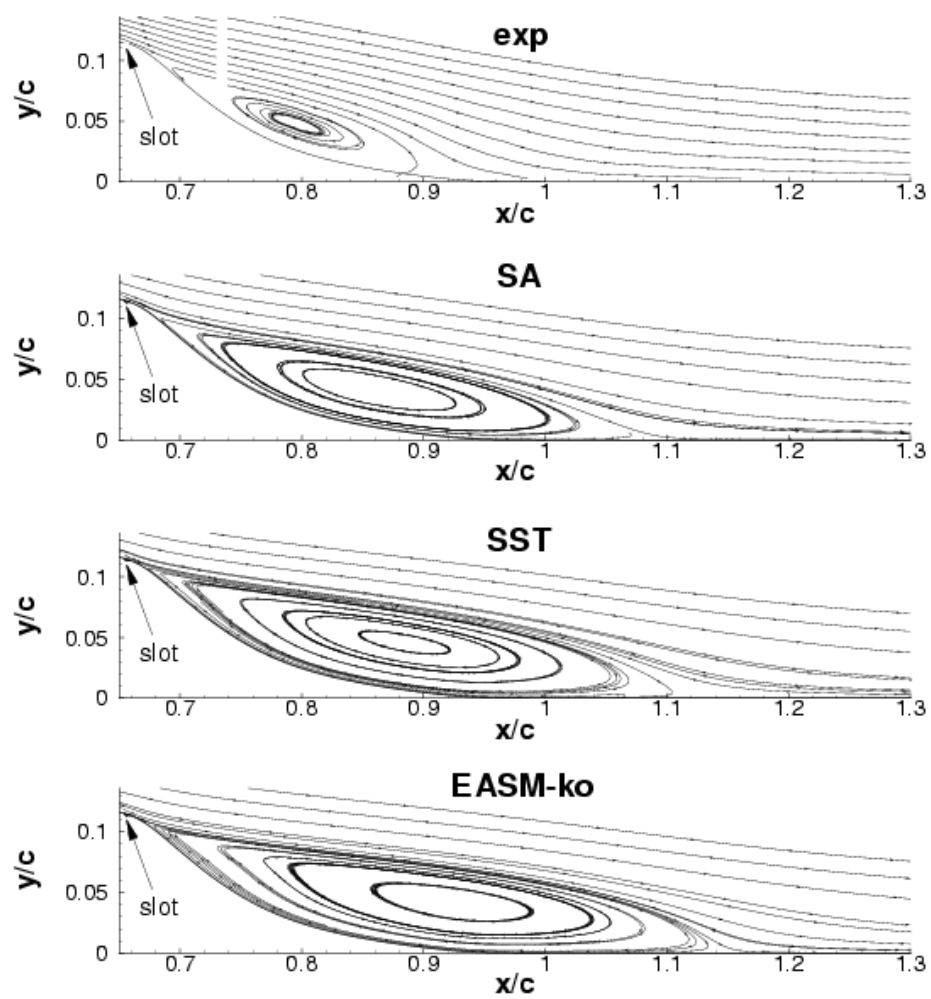
Figure 3. Streamlines for steady suction case, $Re = 0.936$ **million,** $c_\mu = 0.24$**, medium grid.**
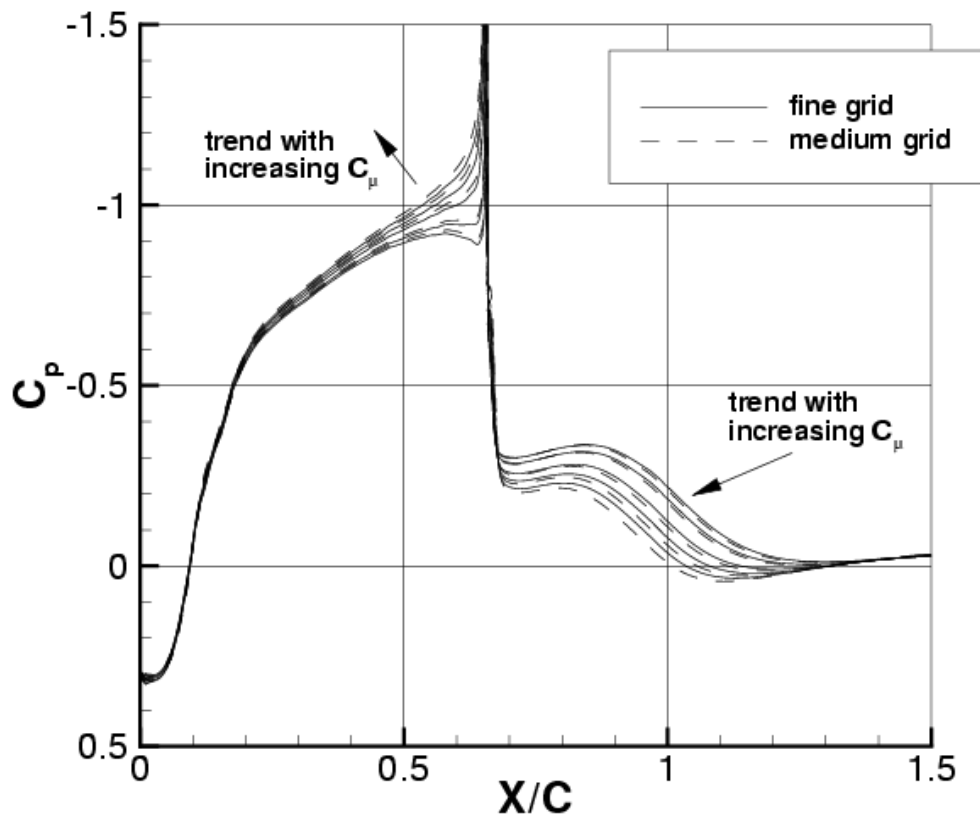
Figure 4. Effect of grid density on surface pressures for steady suction case, $Re = 0.936$ million, c_μ ranging from 0.03 to 0.76; SA model.
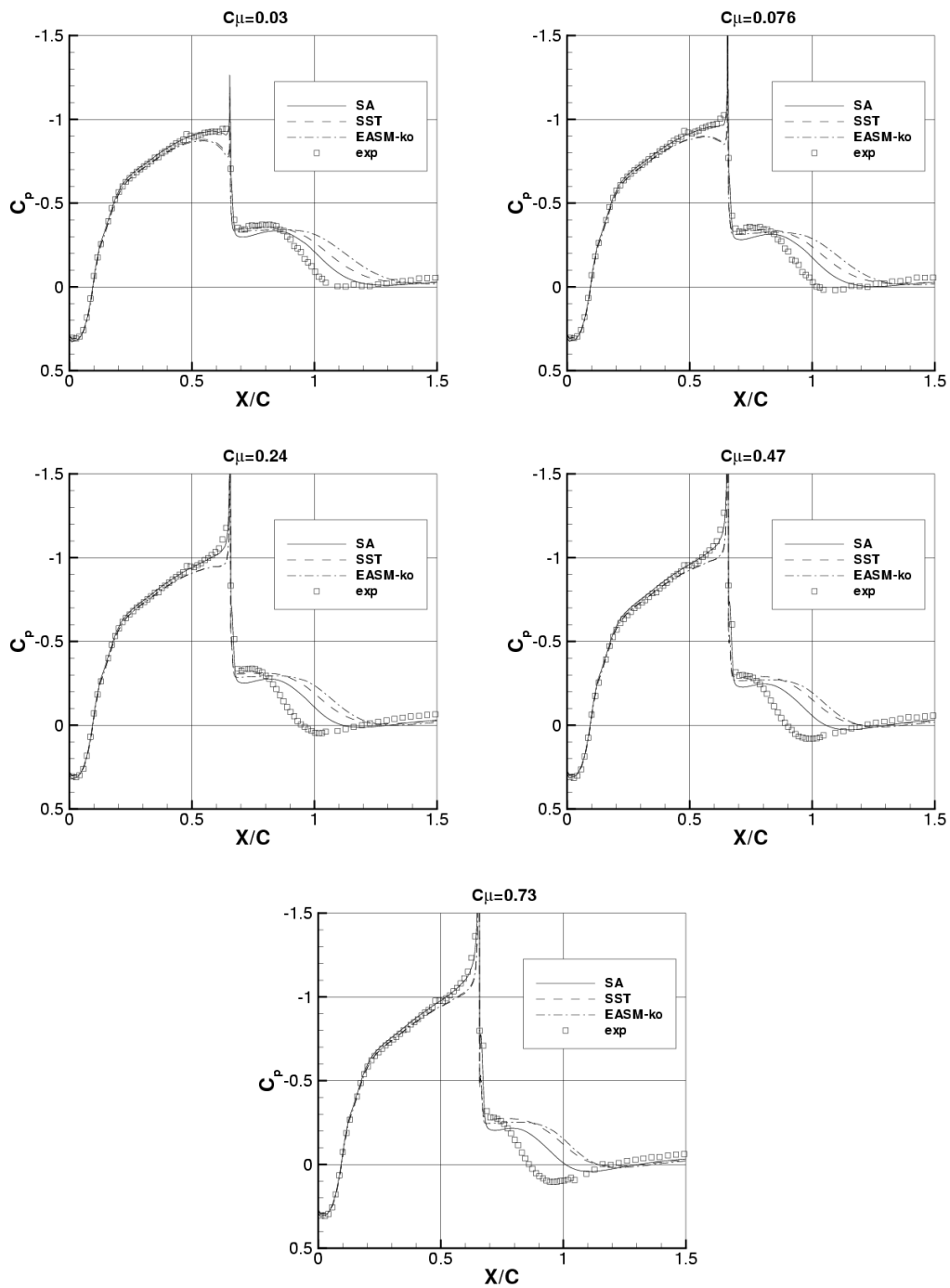
Figure 5. Surface pressure coefficients for steady suction case, $Re = 0.936$ **million, medium grid.**
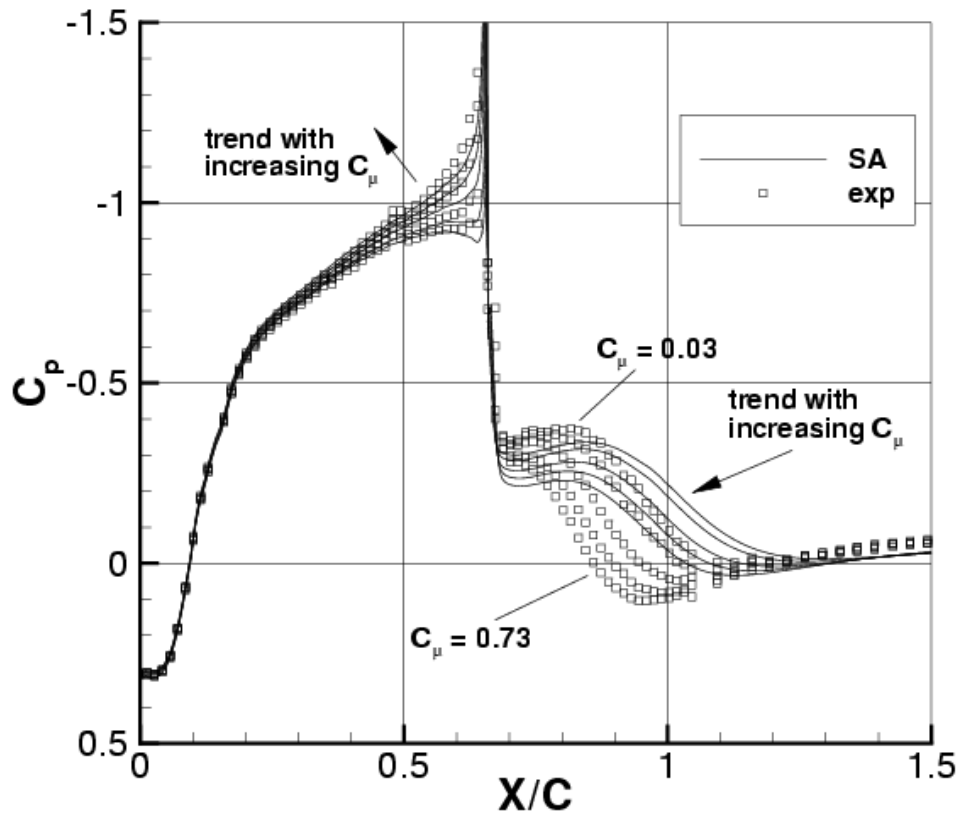
Figure 6. Effect of c_μ on surface pressure coefficients for steady suction, $Re = 0.936$ million, SA model on fine grid.
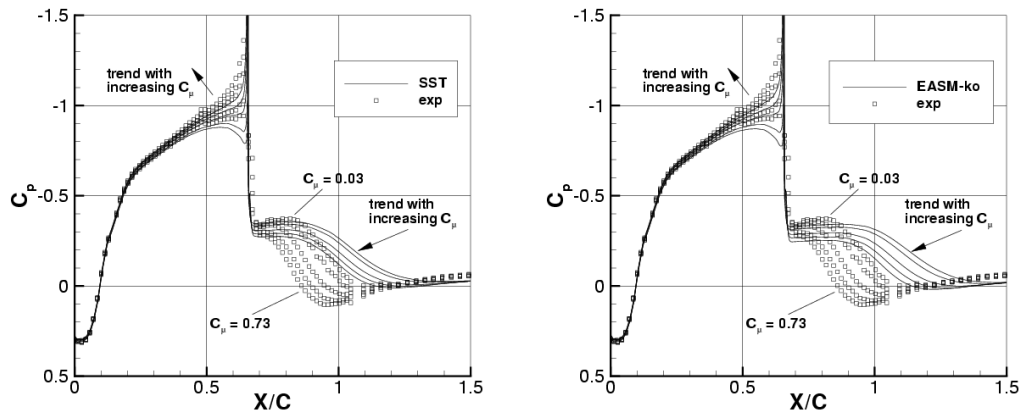
Figure 7. Effect of c_μ on surface pressure coefficients for steady suction, $Re = 0.936$ million, SST (left) and EASM-ko (right) models on medium grid.
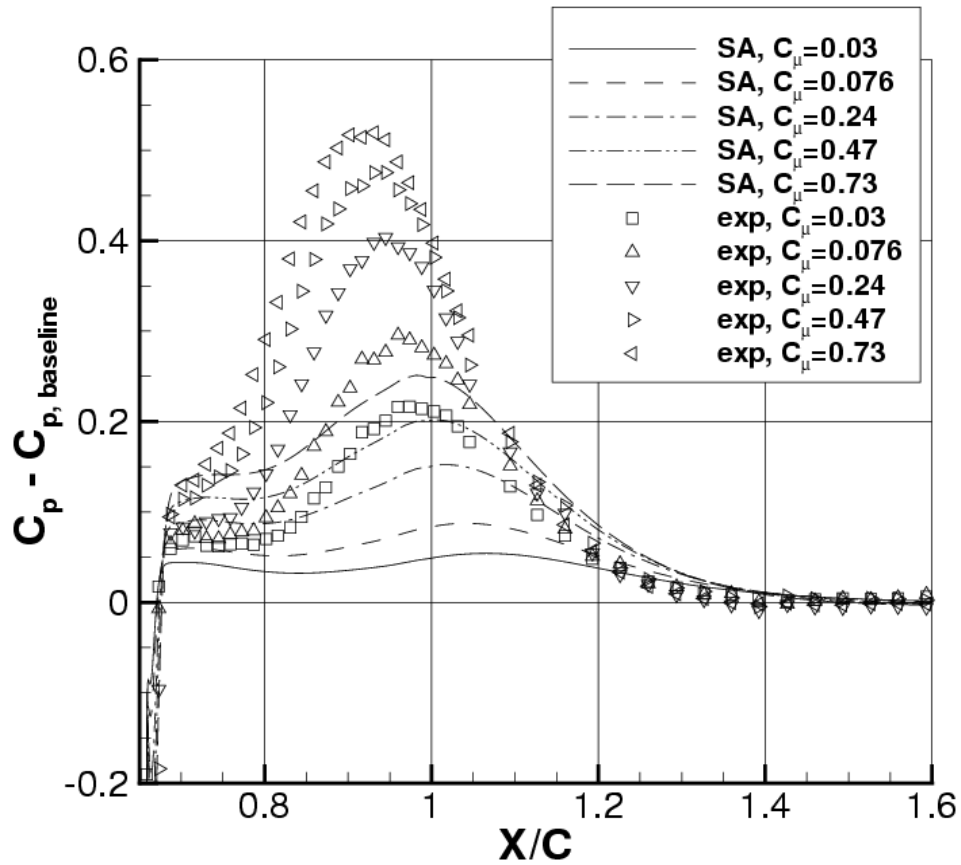
Figure 8. Effect of c_μ on surface pressure coefficients for steady suction relative to baseline (no control), $Re = 0.936$ **million, SA model on medium grid.**
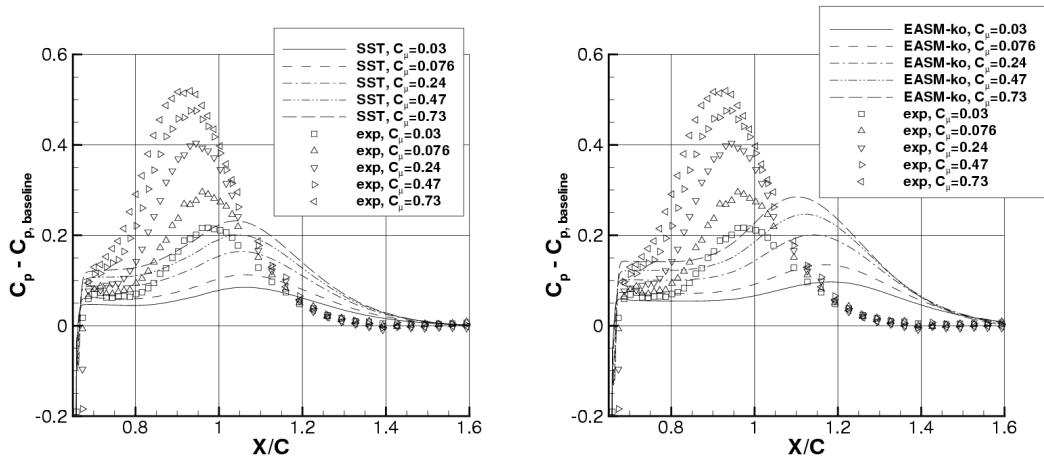
Figure 9. Effect of c_μ on surface pressure coefficients for steady suction relative to baseline (no control), $Re = 0.936$ **million, SST (left) and EASM-ko (right) models on medium grid.**
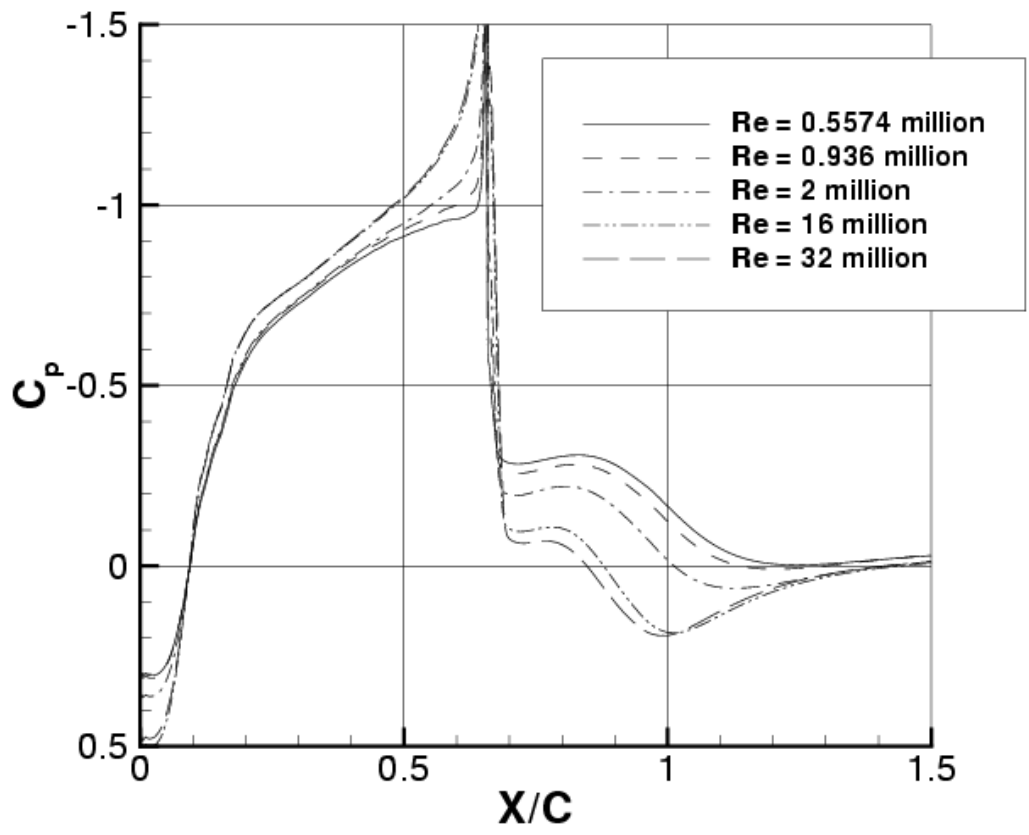
Figure 10. Effect of Reynolds number on surface pressure coefficients for steady suction, $c_\mu = 0.24$; CFD only, SA model on fine grid.
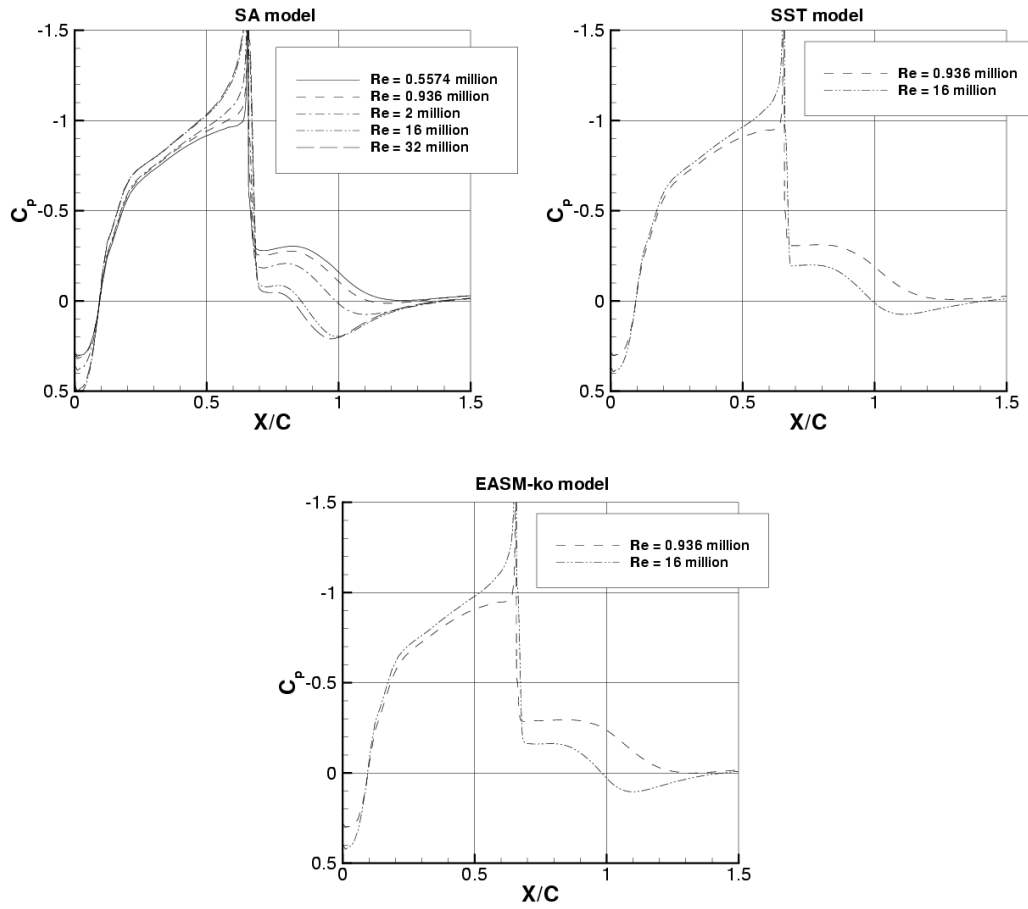
Figure 11. Effect of Reynolds number on surface pressure coefficients for steady suction, $c_\mu = 0.24$; CFD only, all three turbulence models on medium grid.
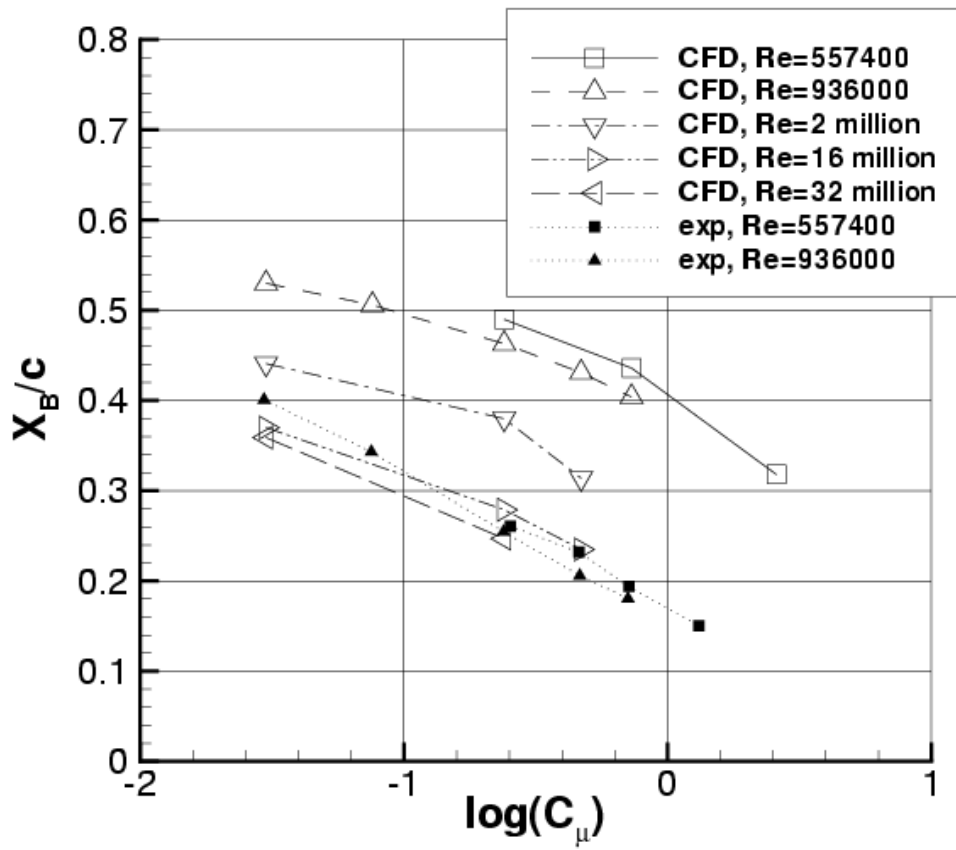
Figure 12. Bubble length as a function of c_μ for steady suction; CFD shows results using SA model, fine grid.
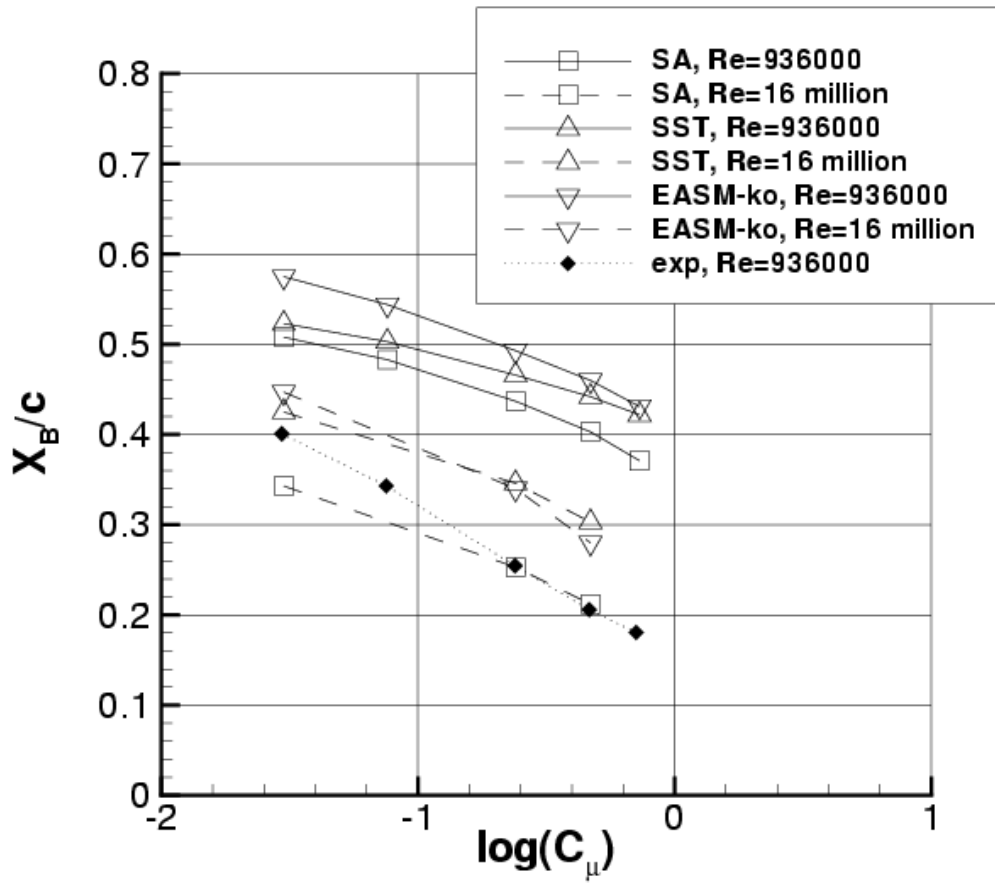
Figure 13. Bubble length as a function of c_μ for steady suction; comparison of different turbulence models, medium grid.
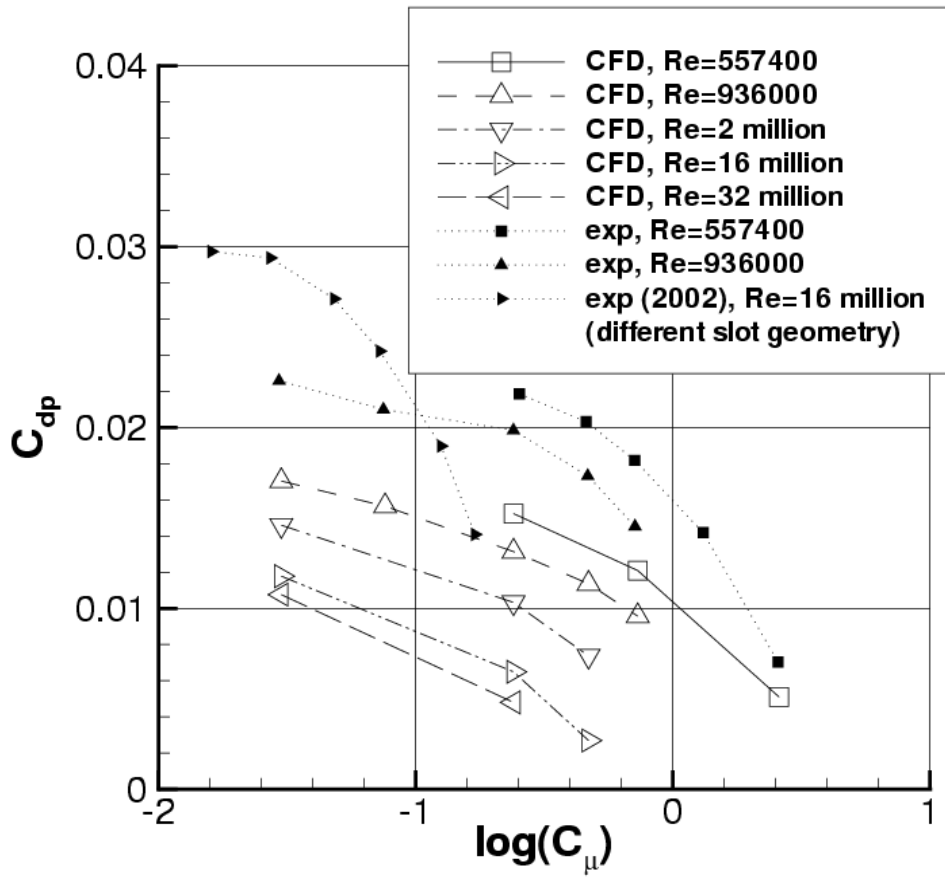
Figure 14. Pressure drag coefficient as a function of c_μ for steady suction; CFD shows results using SA model, fine grid.
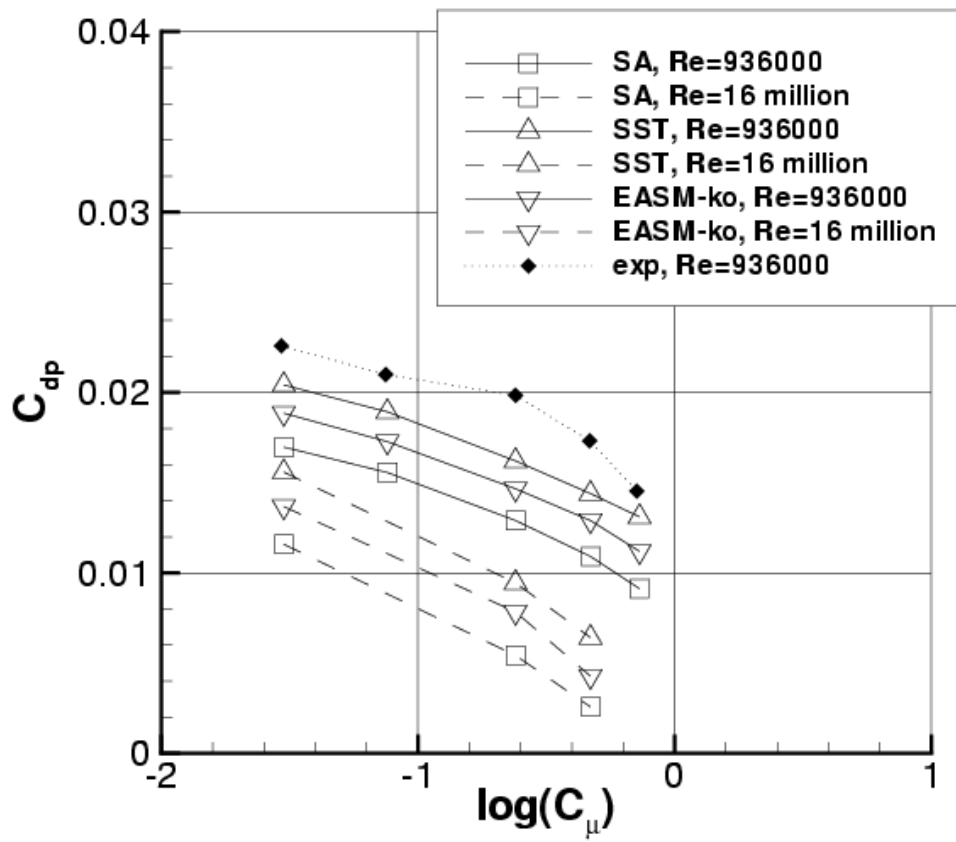
Figure 15. Pressure drag coefficient as a function of c_μ for steady suction; comparison of different turbulence models, medium grid.
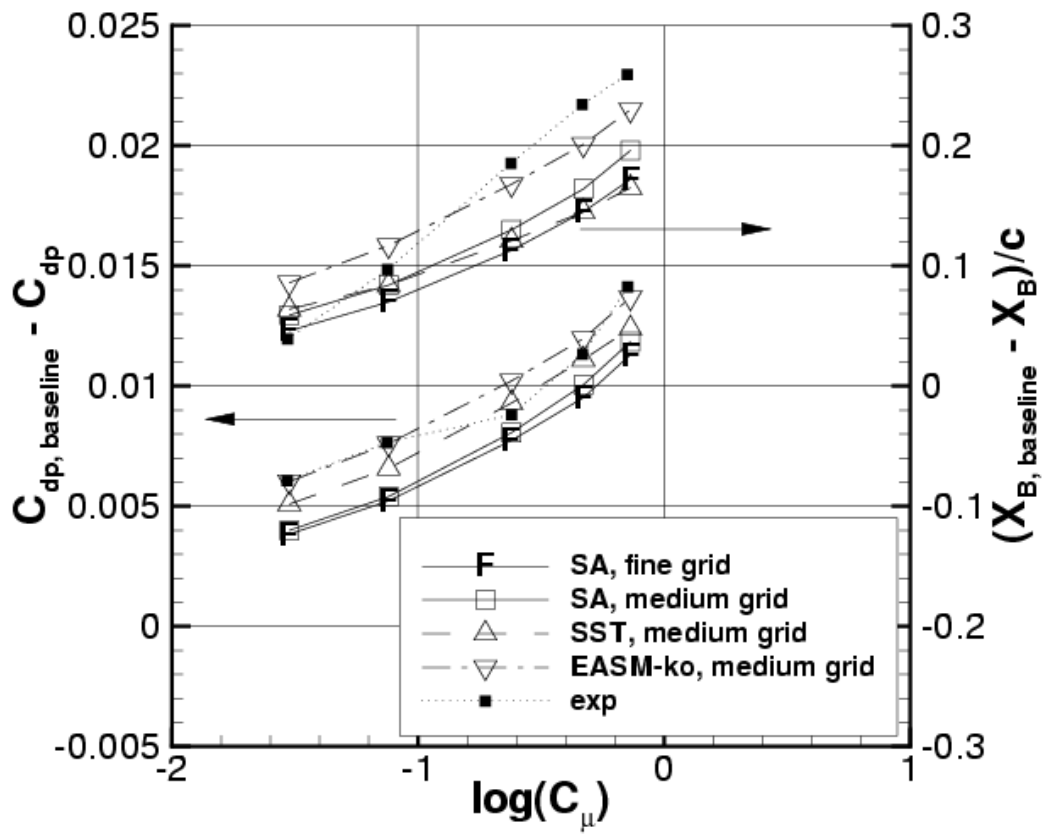
Figure 16. Bubble length and pressure drag coefficient relative to baseline (no control) as a function of c_μ for steady suction, $Re = 0.936$ million.
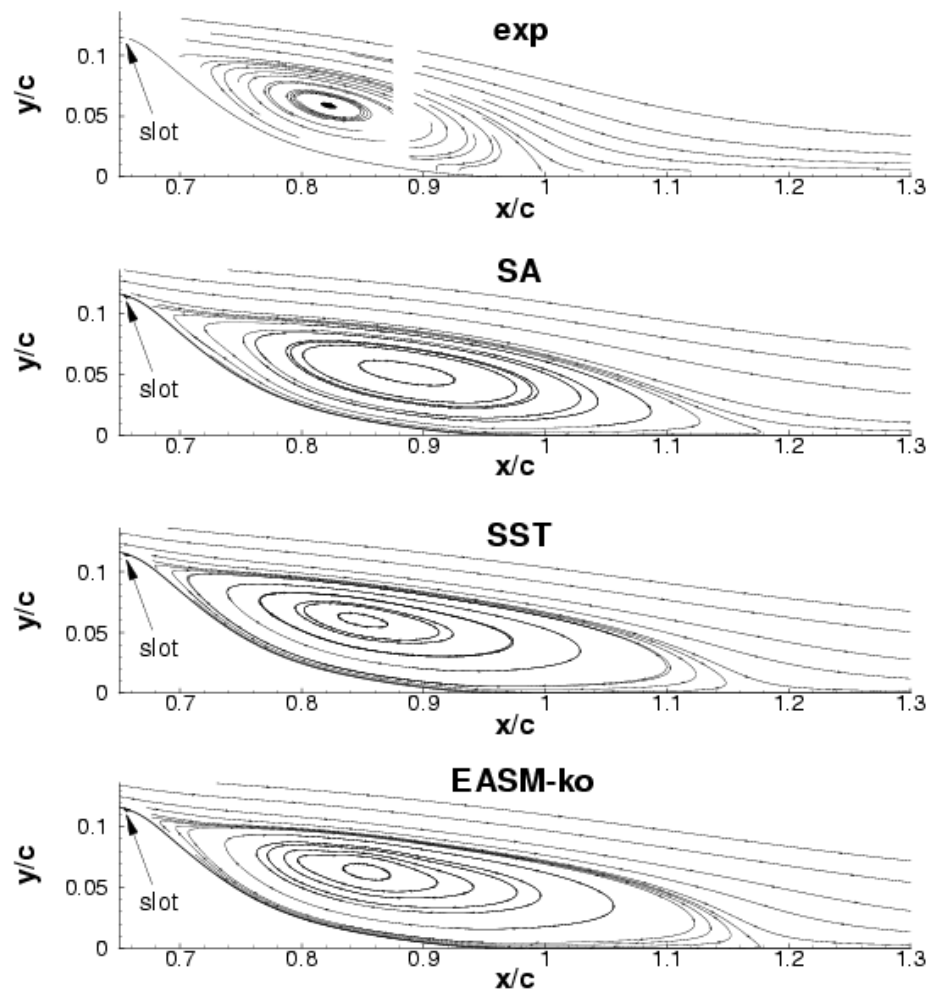
Figure 17. Streamlines for oscillatory control, $Re = 0.936$ **million,** $F^+ = 0.77$, $\langle c_\mu \rangle = 0.11$**%, medium grid.**
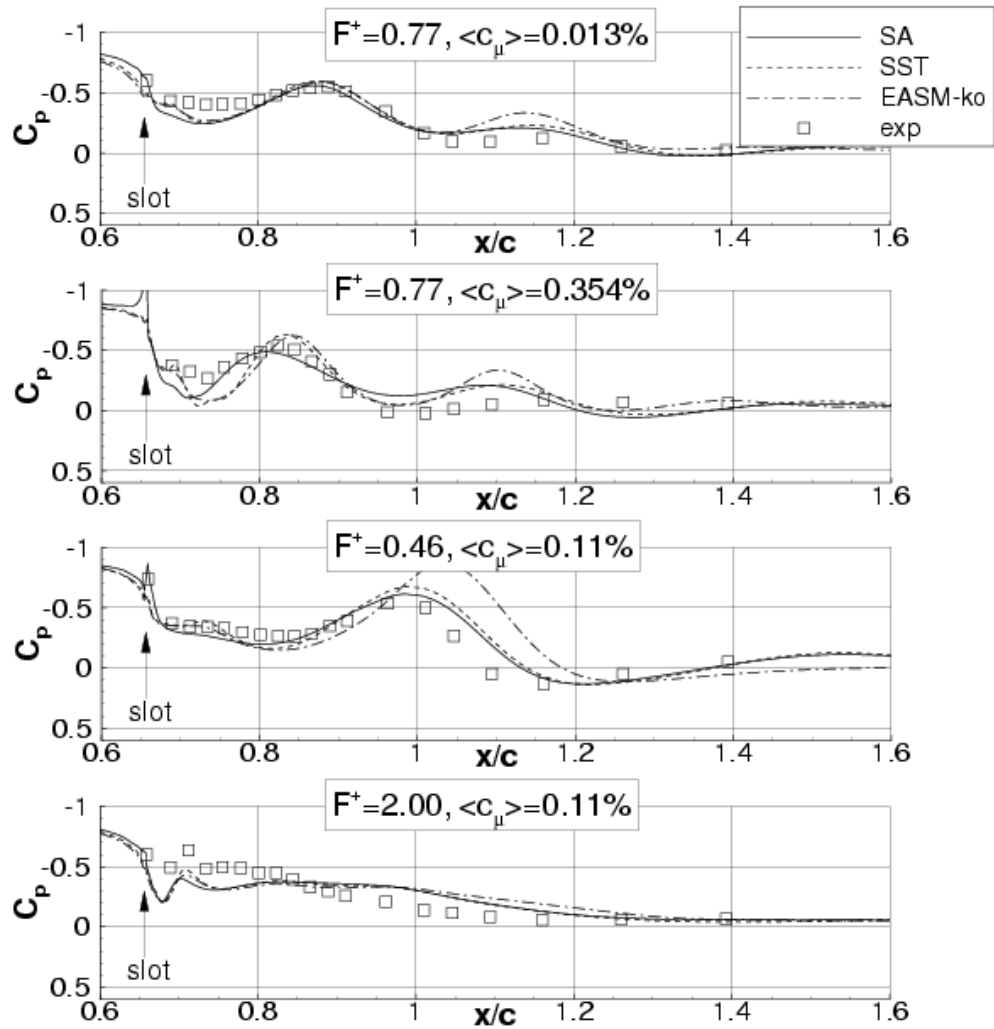
Figure 18. Phase-averaged surface pressure coefficients behind the hump at phase = $80°$ (cycle changing from suction to blowing) for oscillatory control; $Re = 0.936$ million, medium grid.
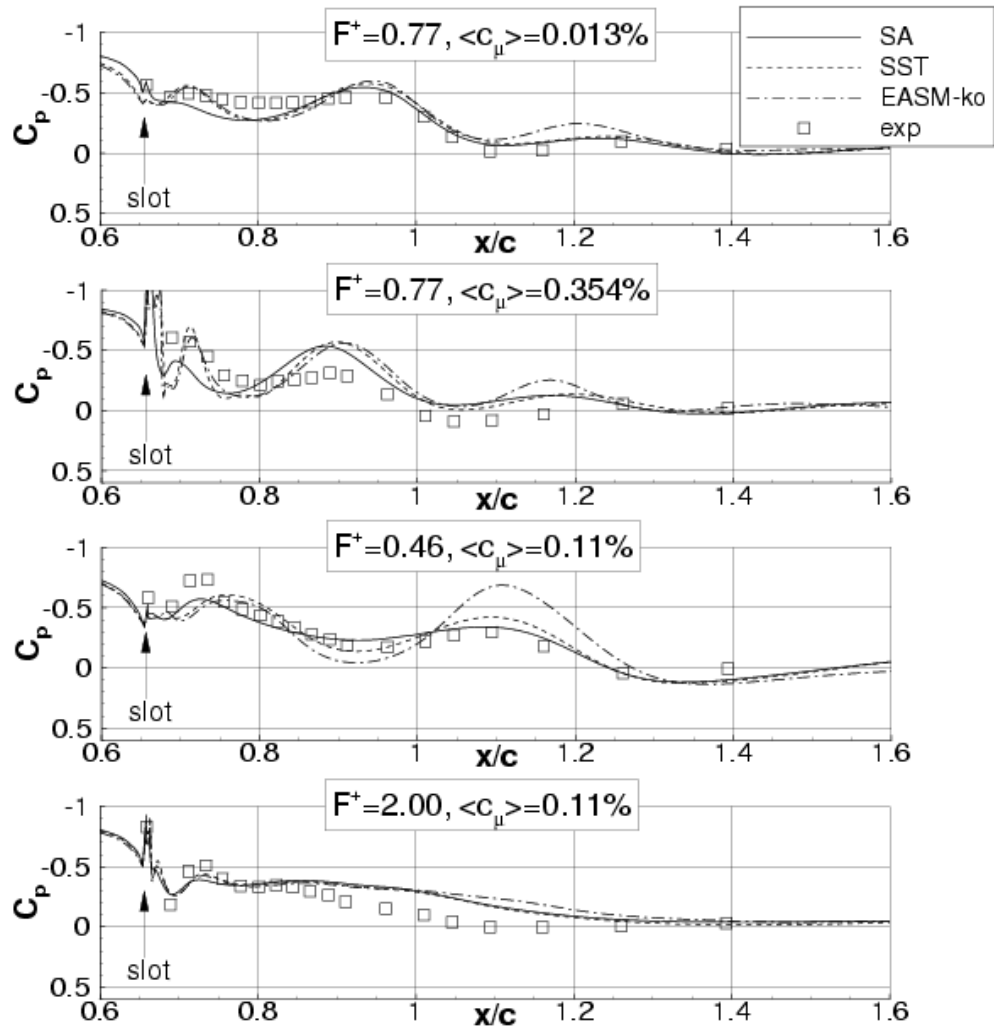
Figure 19. Phase-averaged surface pressure coefficients behind the hump at phase = $170°$ (maximum blowing phase of the cycle) for oscillatory control; $Re = 0.936$ million, medium grid.
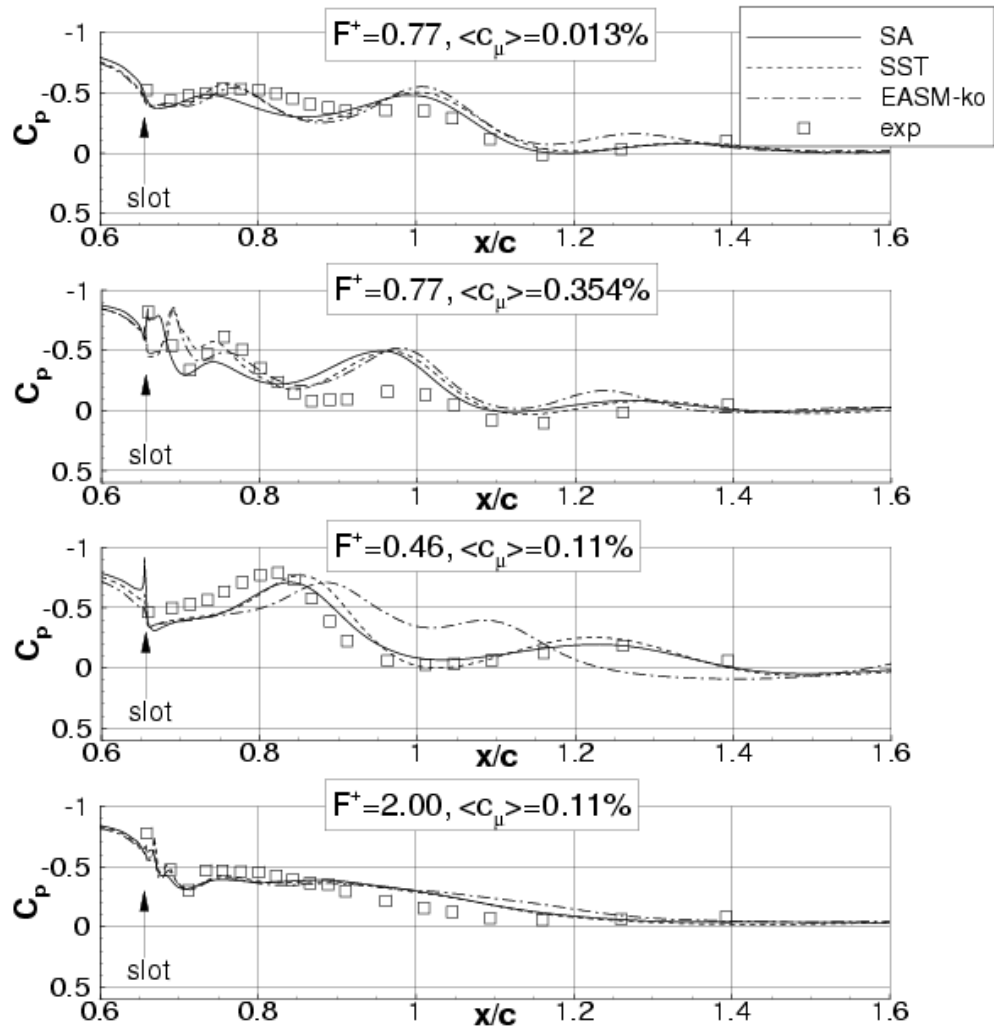
Figure 20. Phase-averaged surface pressure coefficients behind the hump at phase = $260°$ (cycle changing from blowing to suction) for oscillatory control; $Re = 0.936$ million, medium grid.
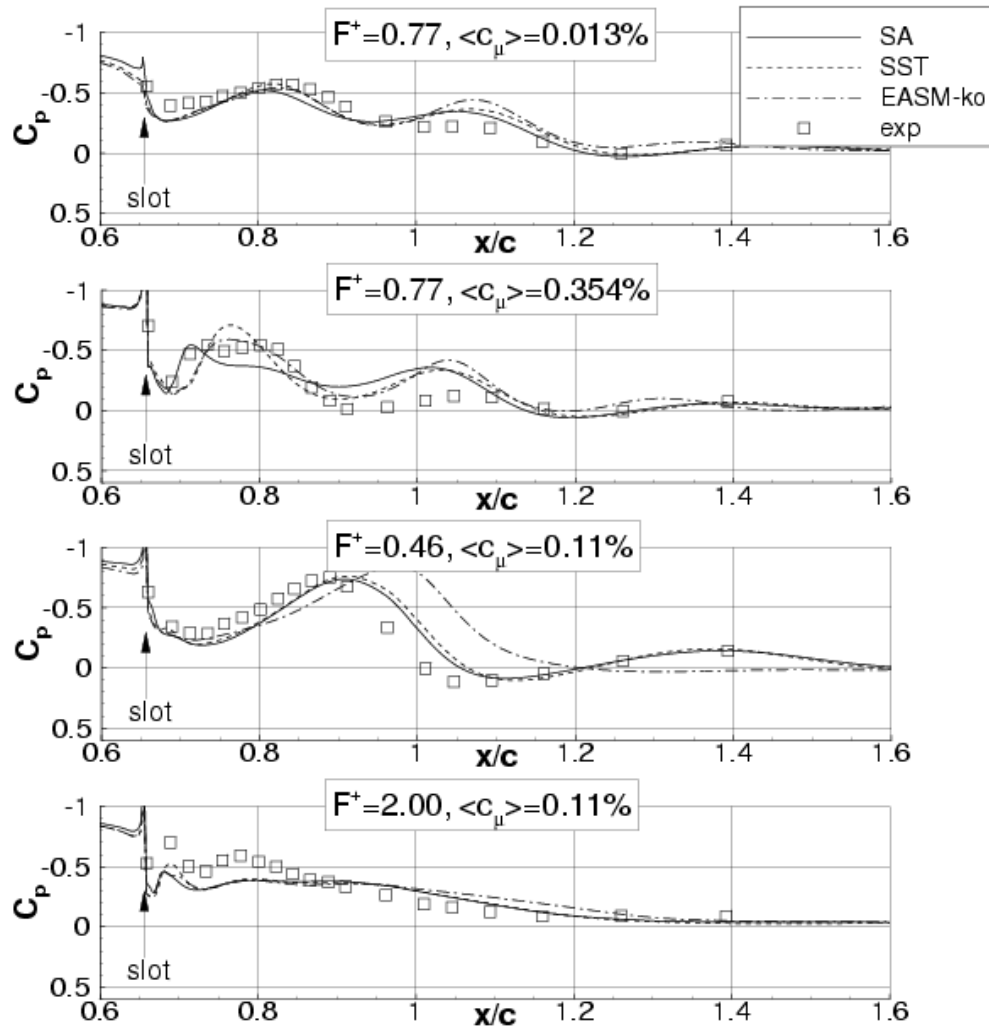
Figure 21. Phase-averaged surface pressure coefficients behind the hump at phase = $350°$ (maximum suction phase of the cycle) for oscillatory control; $Re = 0.936$ million, medium grid.
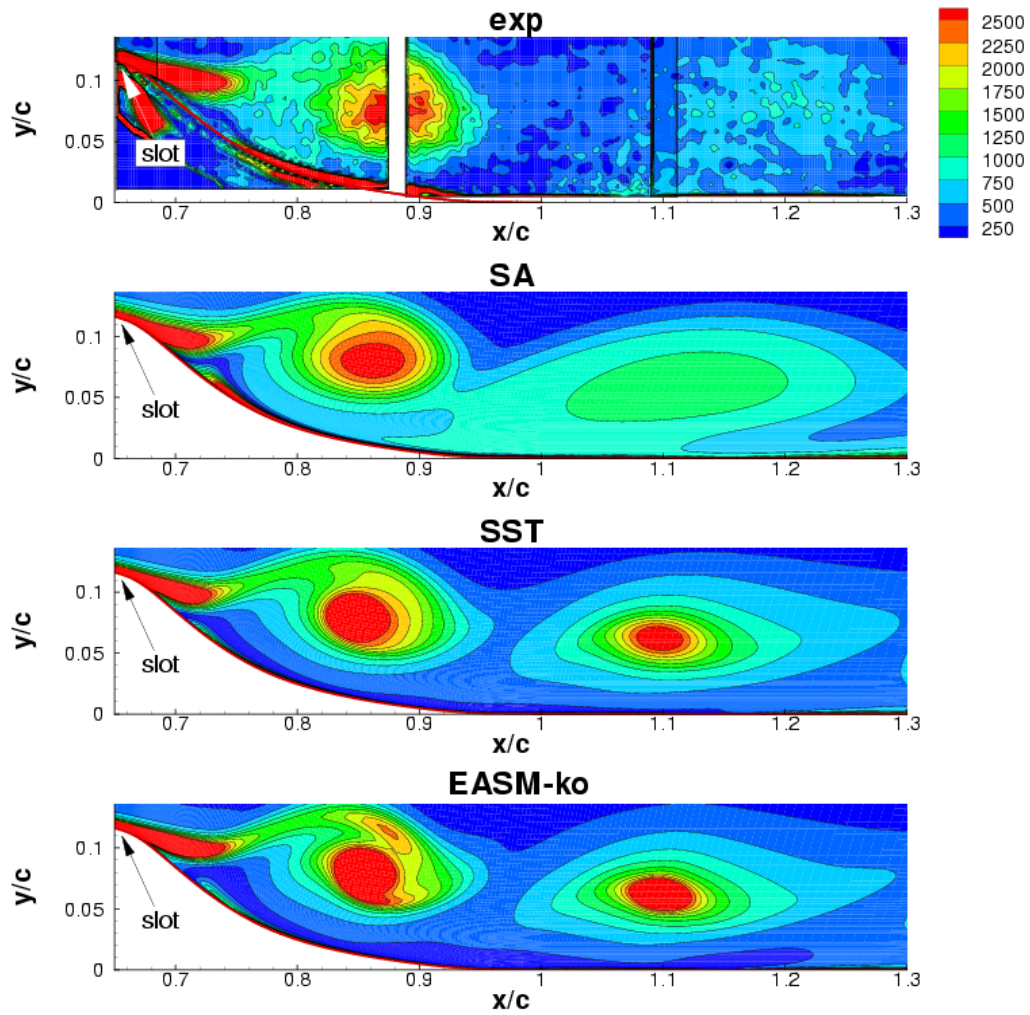
Figure 22. Vorticity contours (in 1/s) at phase = $80°$ (cycle changing from suction to blowing) for oscillatory control; $Re = 0.936$ million, $F^+ = 0.77$, $\langle c_\mu \rangle = 0.11$%, medium grid.
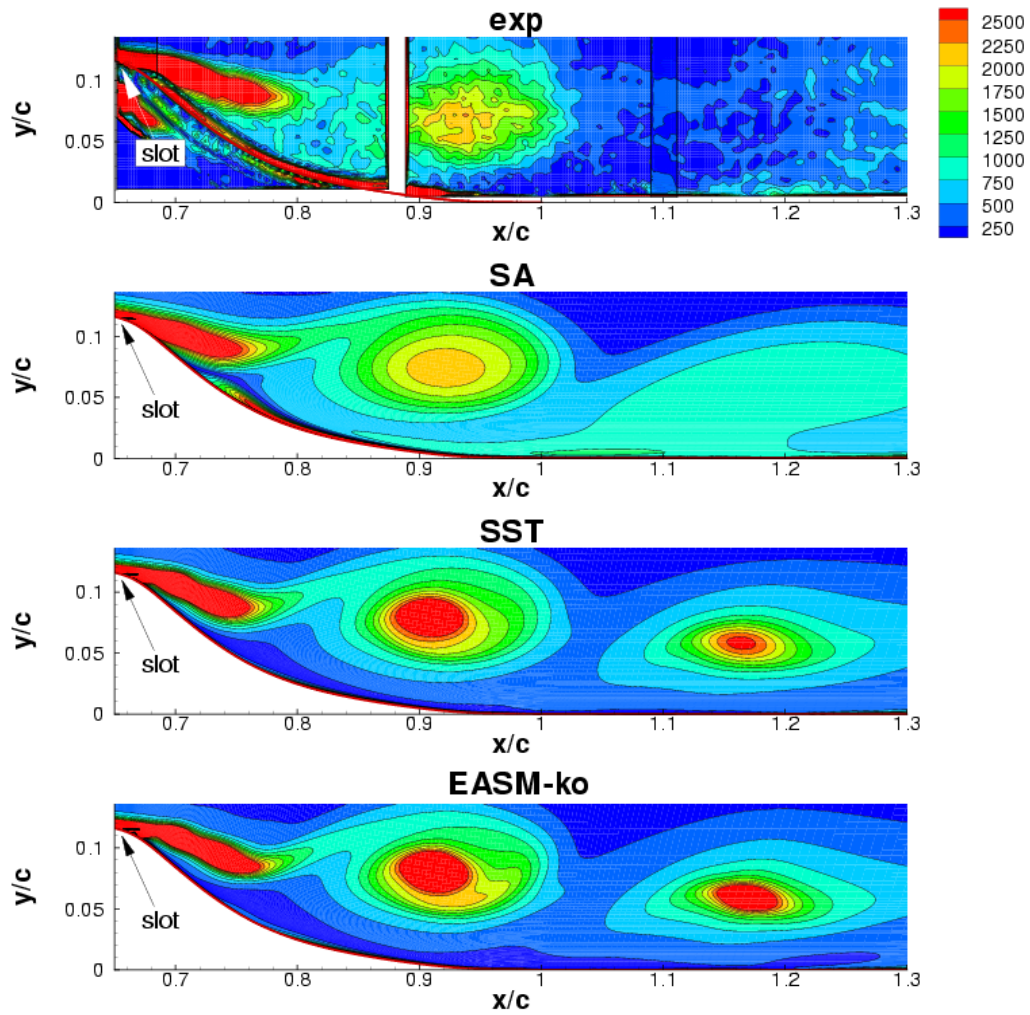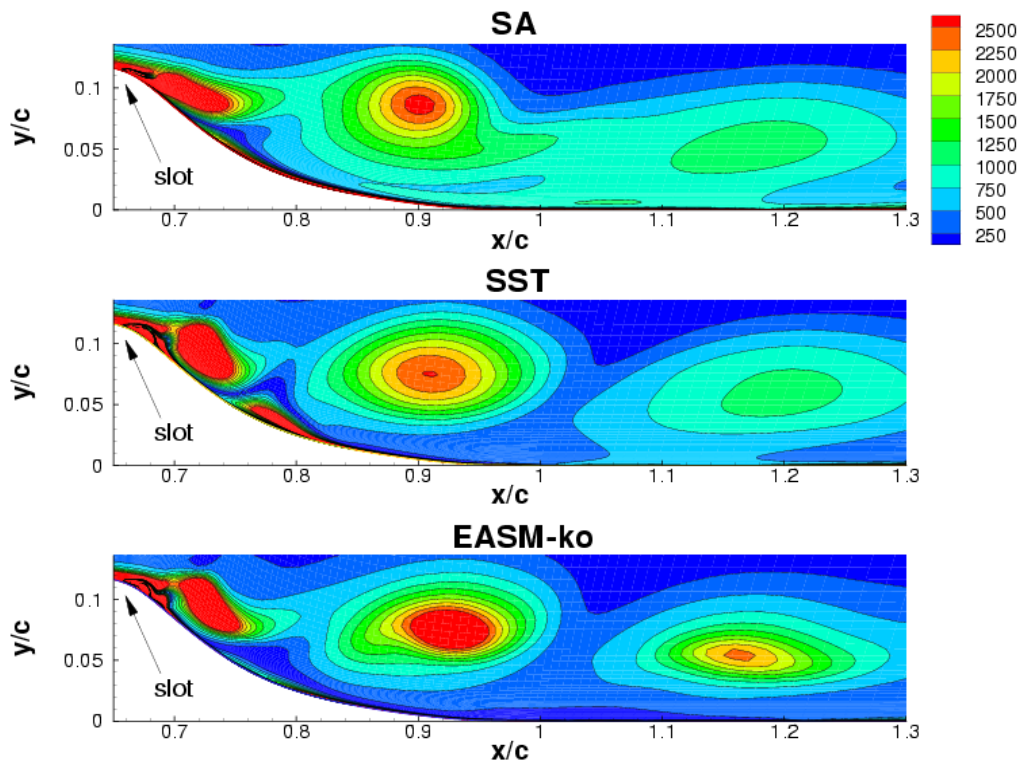
Figure 23. Vorticity contours (in 1/s) at phase = $170°$ (maximum blowing phase of the cycle) for oscillatory control; $Re = 0.936$ million, $F^+ = 0.77$, $\langle c_\mu \rangle = 0.11$%, medium grid.
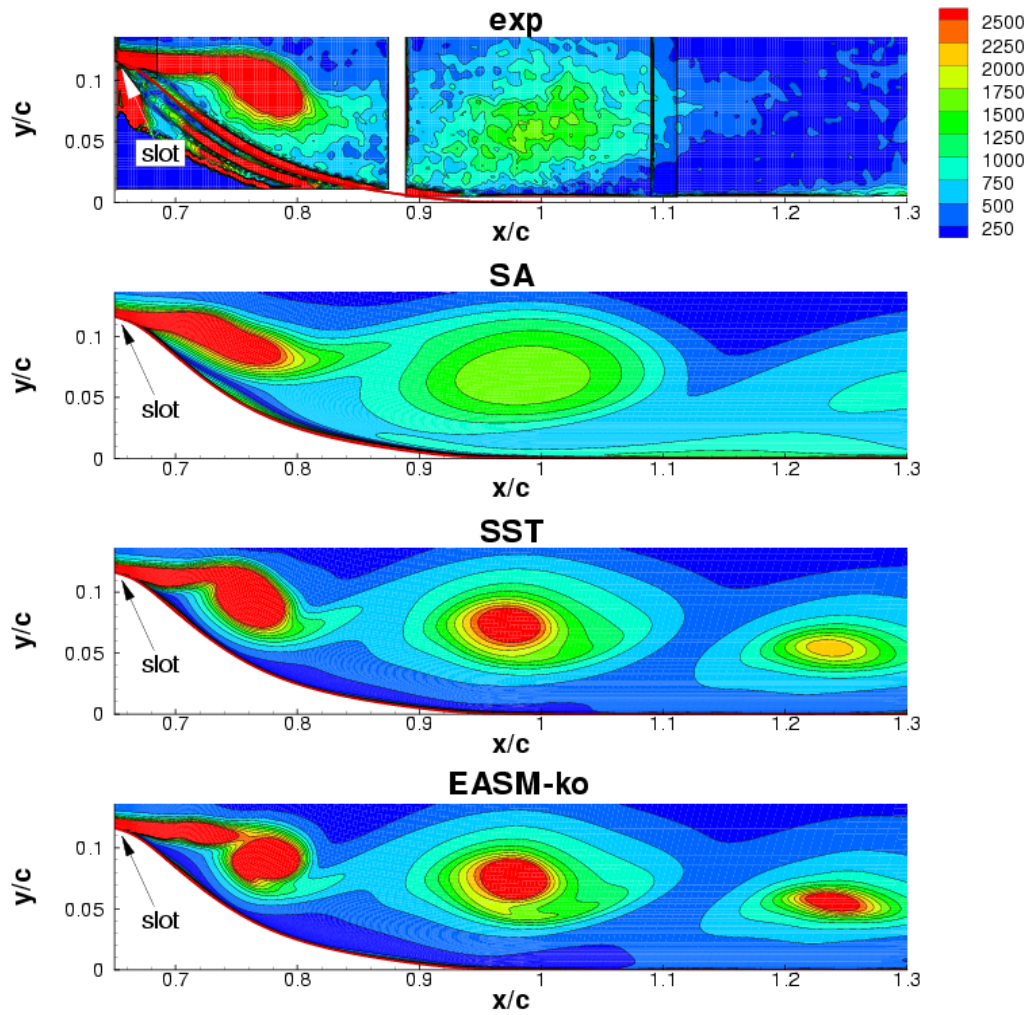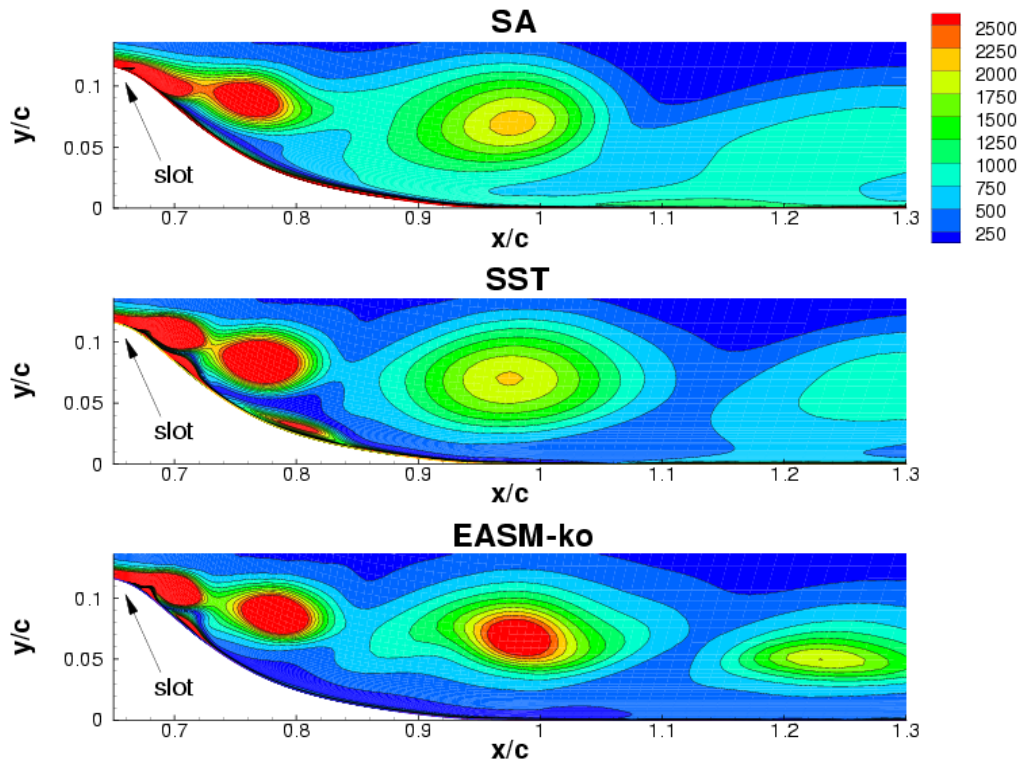
Figure 24. Vorticity contours (in 1/s) at phase = $260°$ (cycle changing from blowing to suction) for oscillatory control; $Re = 0.936$ **million,** $F^+ = 0.77$, $\langle c_\mu \rangle = 0.11$**%, medium grid.**
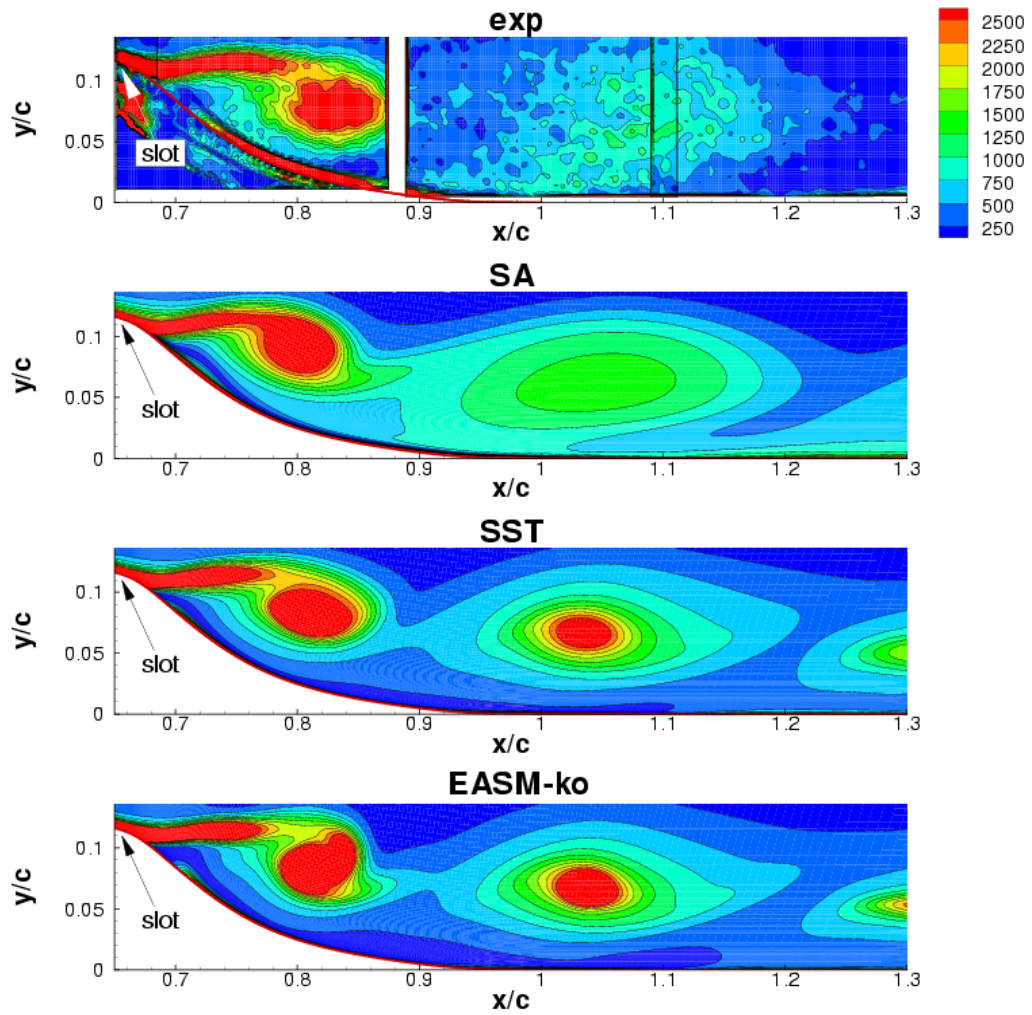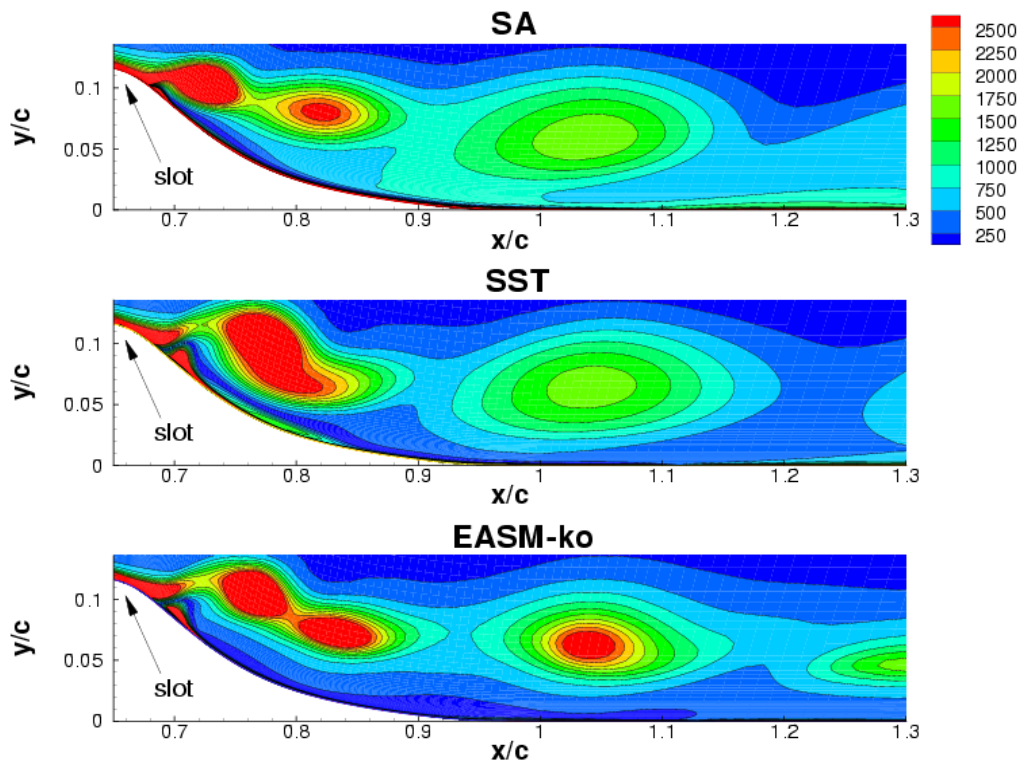
Figure 25. Vorticity contours (in 1/s) at phase = $350°$ (maximum suction phase of the cycle) for oscillatory control; $Re = 0.936$ **million,** $F^+ = 0.77$, $\langle c_\mu \rangle = 0.11$**%, medium grid.**
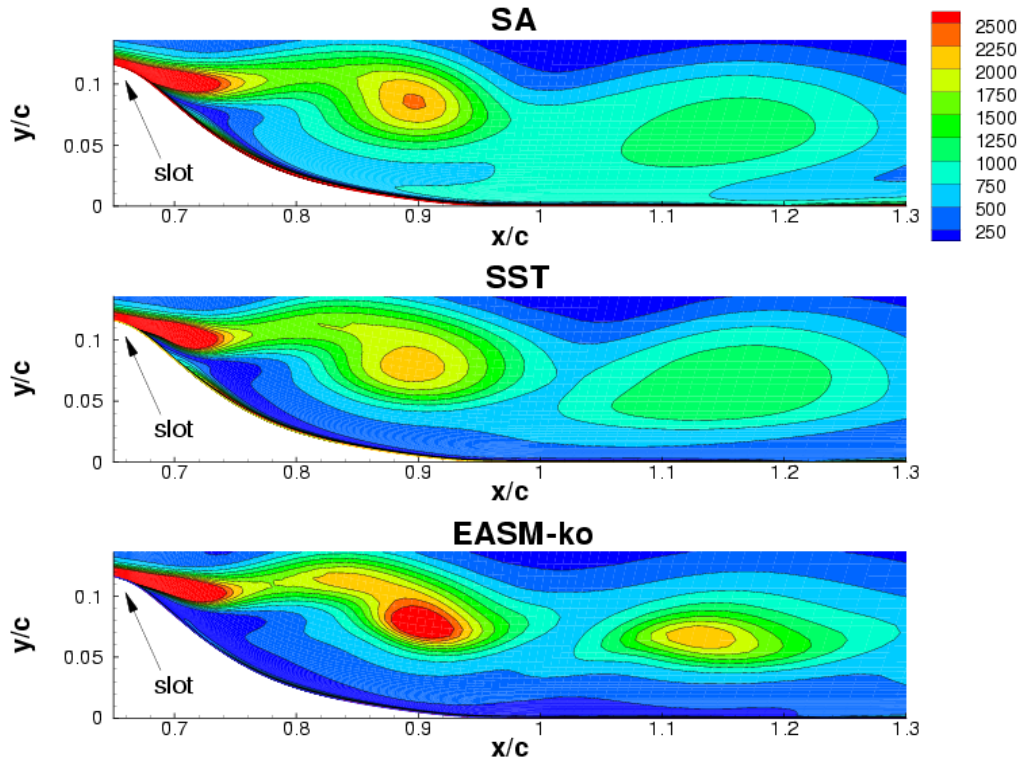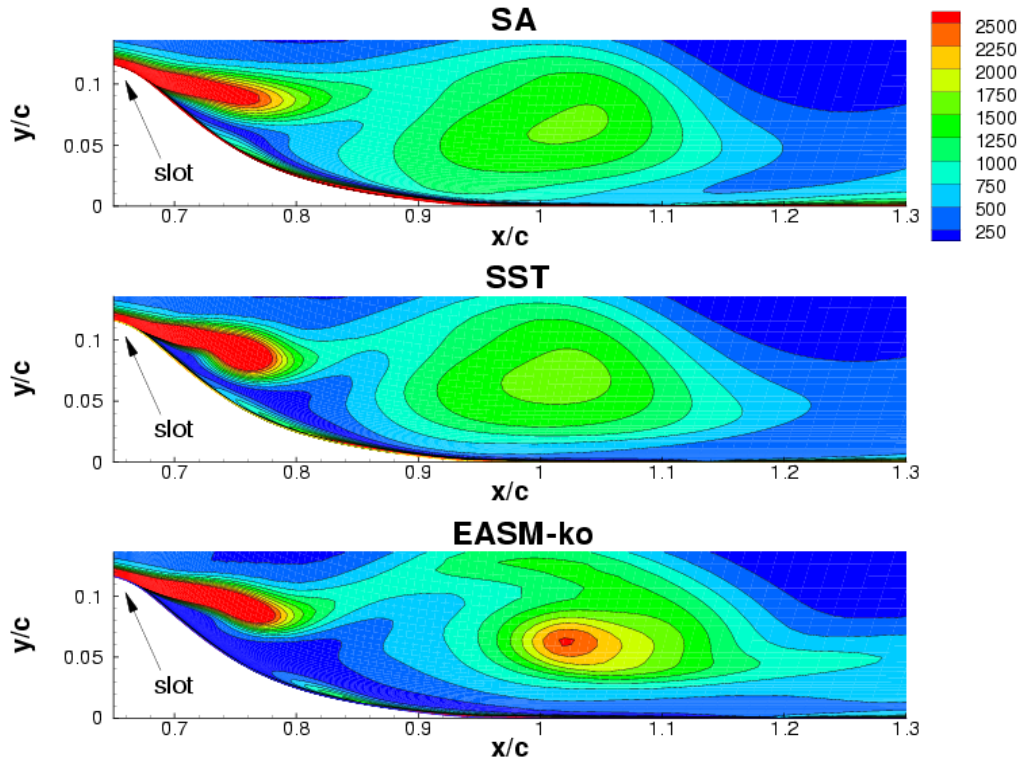
Figure 26. Vorticity contours (in 1/s) for lower $\langle c_\mu \rangle$ than workshop case, at phase = $80°$ (cycle changing from suction to blowing) for oscillatory control; $Re = 0.936$ **million,** $F^+ = 0.77$, $\langle c_\mu \rangle = 0.013$**%, medium grid.**
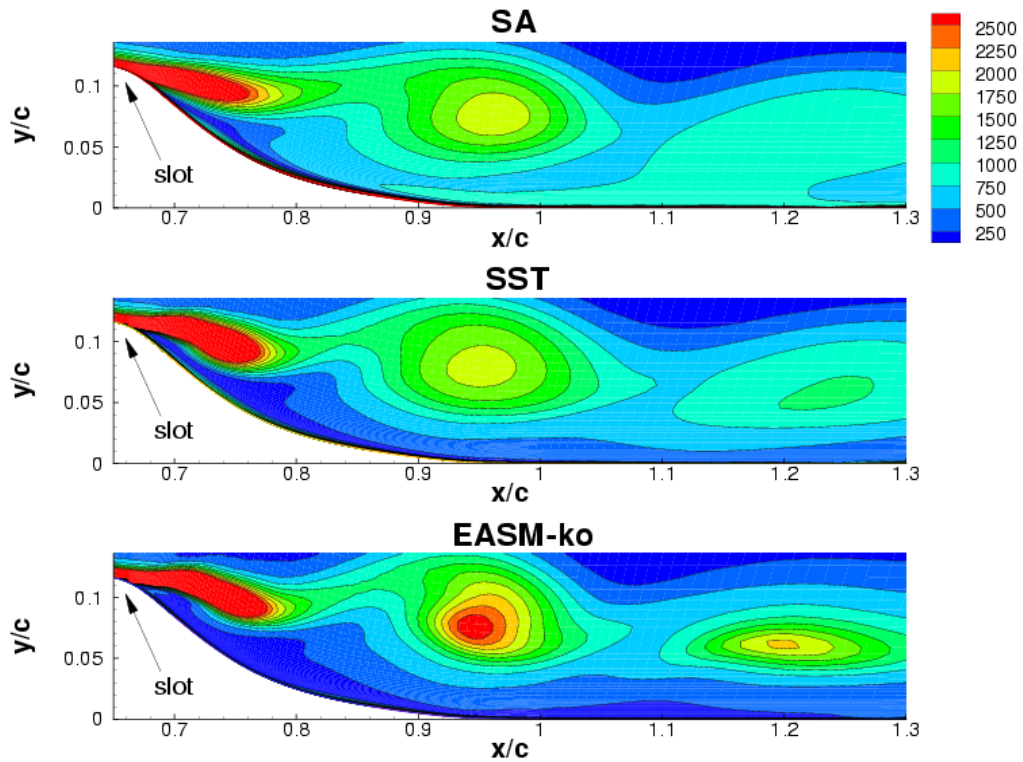
Figure 27. Vorticity contours (in 1/s) for lower $\langle c_\mu \rangle$ than workshop case, at phase = $170°$ **(maximum blowing phase of the cycle) for oscillatory control;** $Re = 0.936$ **million,** $F^+ = 0.77$, $\langle c_\mu \rangle = 0.013$**%, medium grid.**
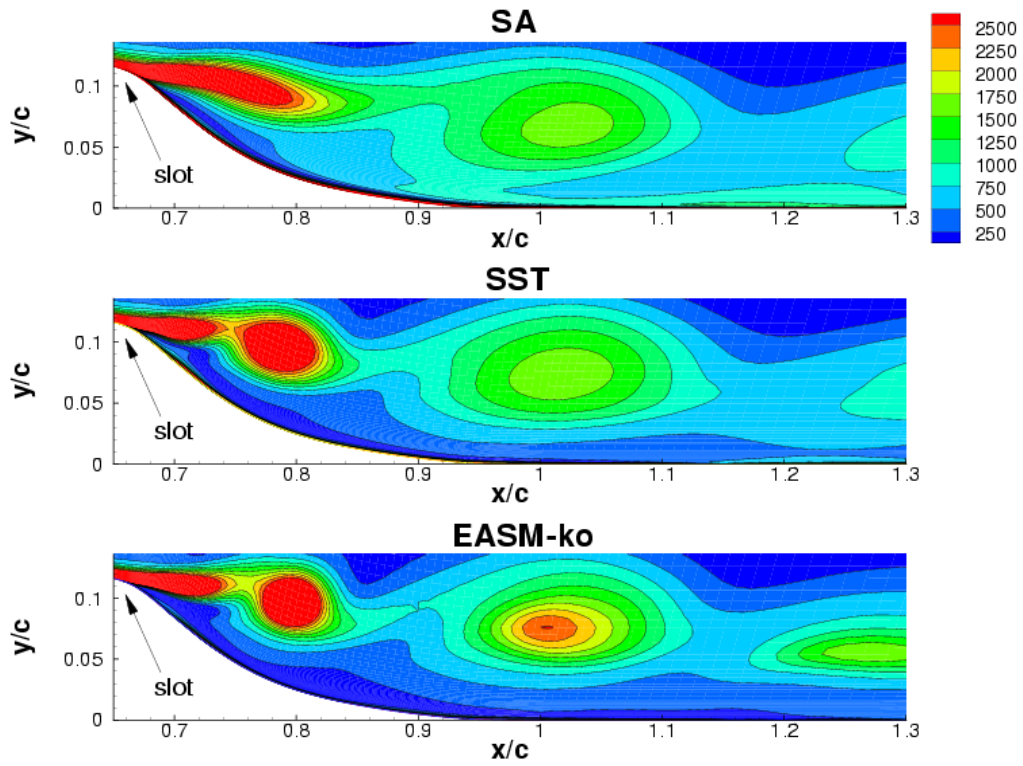
Figure 28. Vorticity contours (in 1/s) for lower $\langle c_\mu \rangle$ than workshop case, at phase $= 260°$ (cycle changing from blowing to suction) for oscillatory control; $Re = 0.936$ million, $F^+ = 0.77$, $\langle c_\mu \rangle = 0.013$%, medium grid.
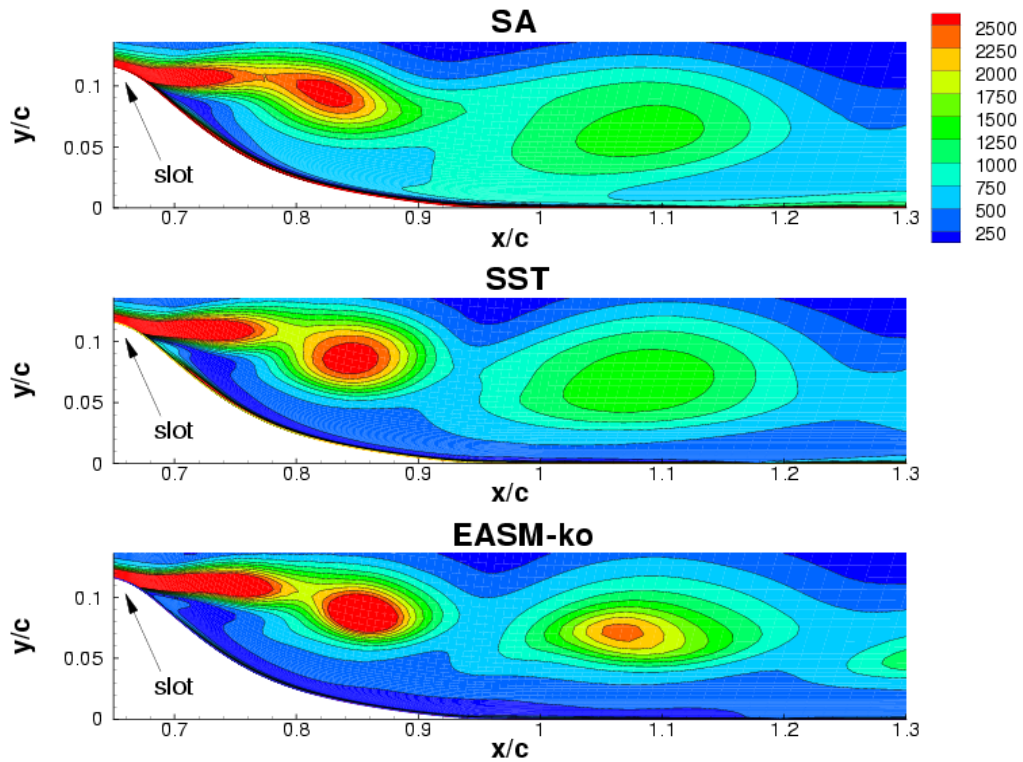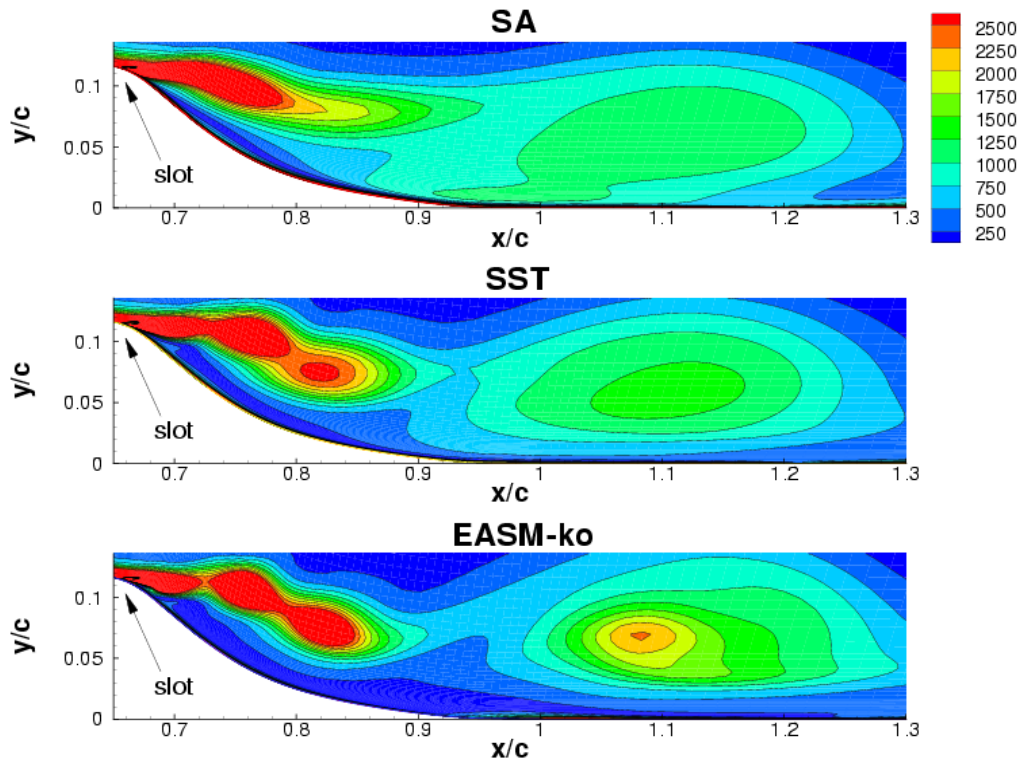

Figure 29. Vorticity contours (in 1/s) for lower $\langle c_\mu \rangle$ than workshop case, at phase $= 350°$ (maximum suction phase of the cycle) for oscillatory control; $Re = 0.936$ million, $F^+ = 0.77$, $\langle c_\mu \rangle = 0.013$%, medium grid.
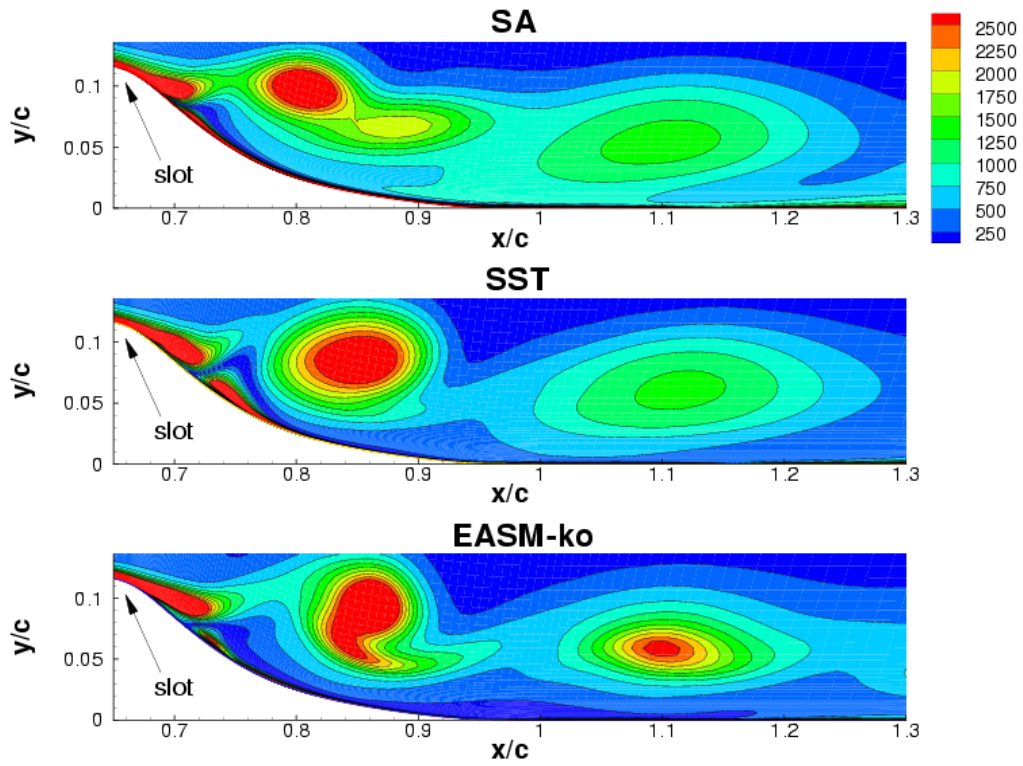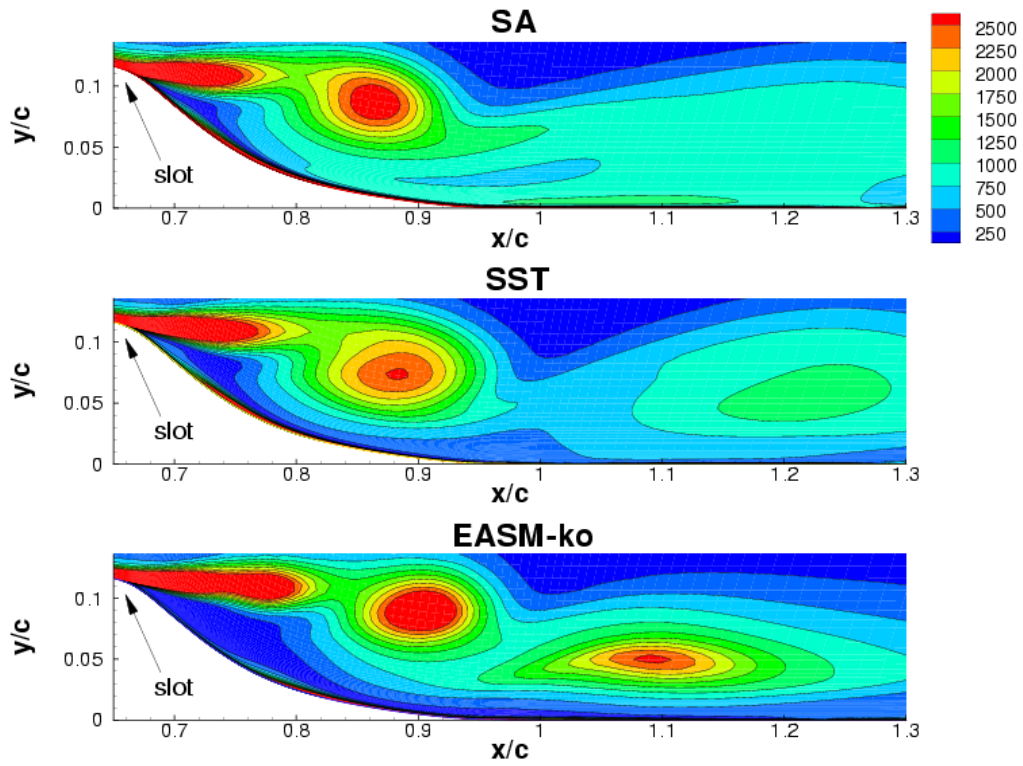
Figure 30. Vorticity contours (in 1/s) for higher $\langle c_\mu \rangle$ than workshop case, at phase = $80°$ (cycle changing from suction to blowing) for oscillatory control; $Re = 0.936$ million, $F^+ = 0.77$, $\langle c_\mu \rangle = 0.354$%, medium grid.

Figure 31. Vorticity contours (in 1/s) for higher $\langle c_\mu \rangle$ than workshop case, at phase = $170°$ (maximum blowing phase of the cycle) for oscillatory control; $Re = 0.936$ million, $F^+ = 0.77$, $\langle c_\mu \rangle = 0.354$%, medium grid.

Figure 32. Vorticity contours (in 1/s) for higher $\langle c_\mu \rangle$ than workshop case, at phase $= 260°$ (cycle changing from blowing to suction) for oscillatory control; $Re = 0.936$ million, $F^+ = 0.77$, $\langle c_\mu \rangle = 0.354$%, medium grid.
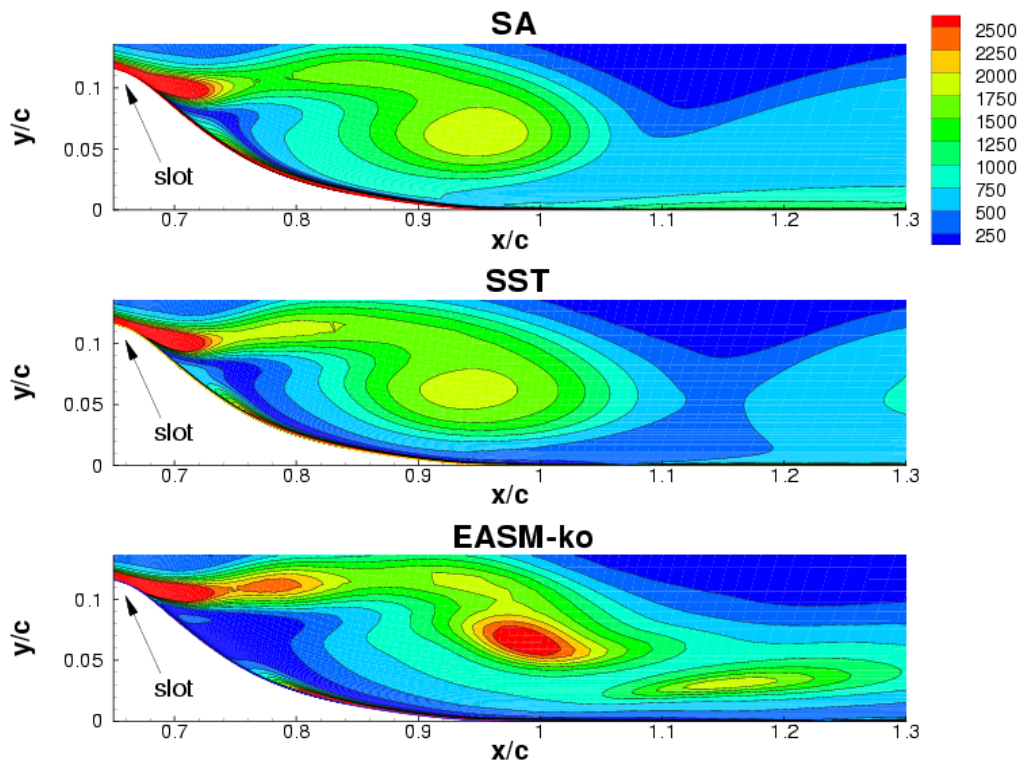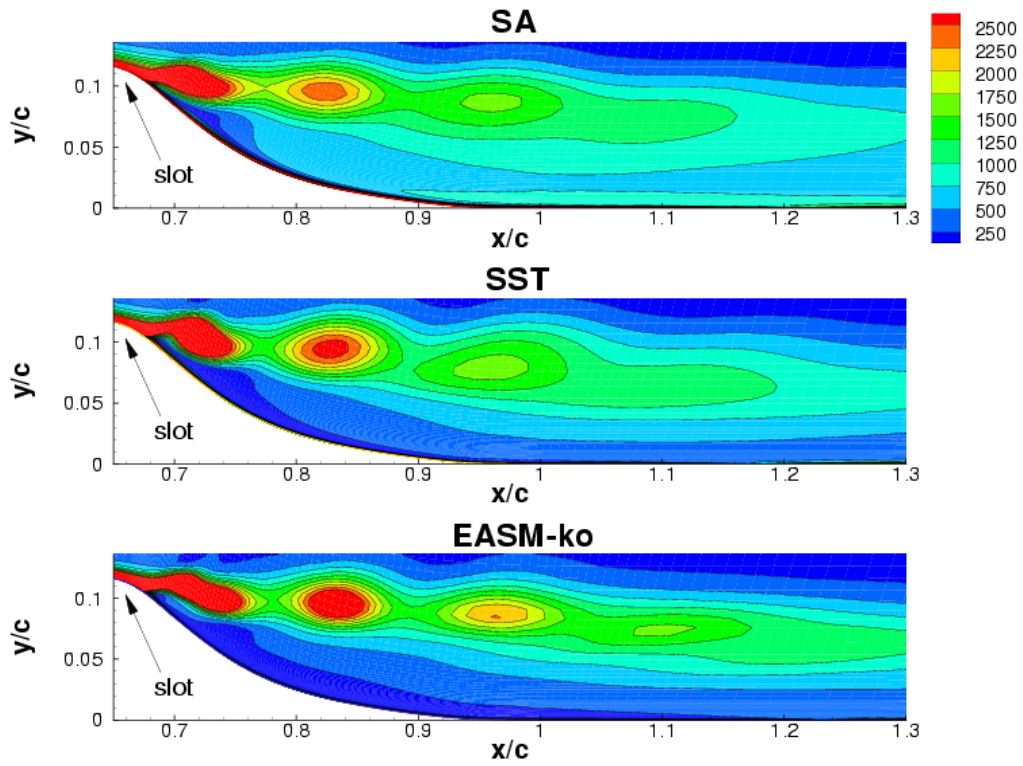

Figure 33. Vorticity contours (in 1/s) for higher $\langle c_\mu \rangle$ than workshop case, at phase $= 350°$ (maximum suction phase of the cycle) for oscillatory control; $Re = 0.936$ million, $F^+ = 0.77$, $\langle c_\mu \rangle = 0.354$%, medium grid.

Figure 34. Vorticity contours (in 1/s) for lower F^+ than workshop case, at phase $= 80°$ (cycle changing from suction to blowing) for oscillatory control; $Re = 0.936$ million, $F^+ = 0.46$, $\langle c_\mu \rangle = 0.11$%, medium grid.
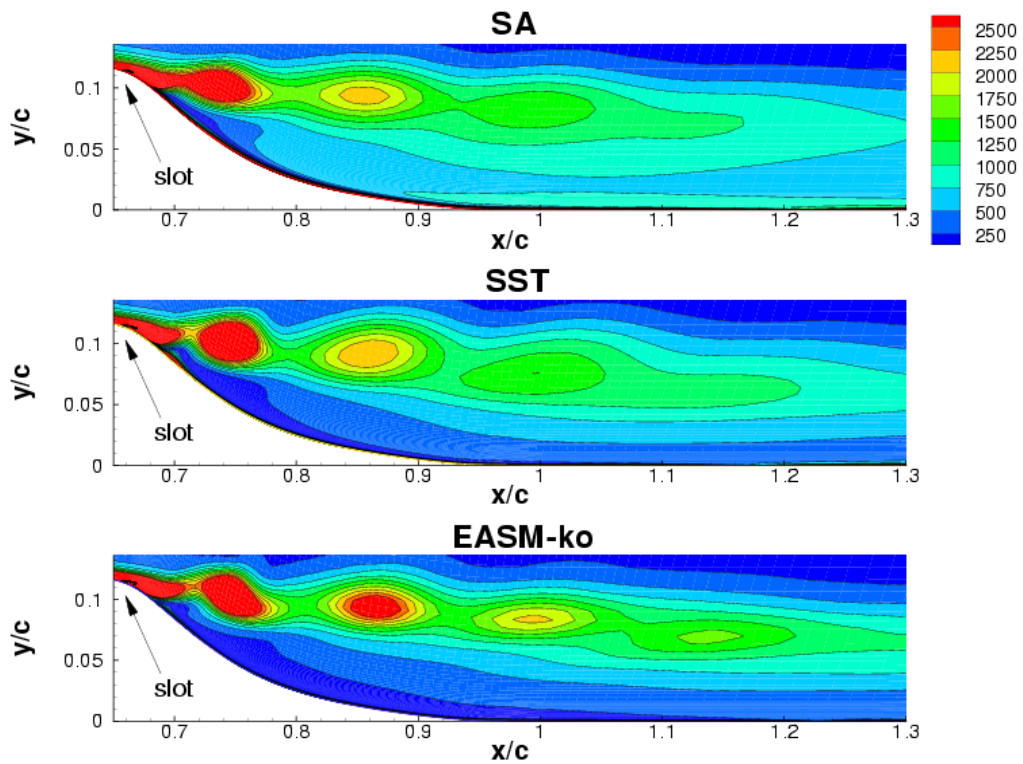

Figure 35. Vorticity contours (in 1/s) for lower F^+ than workshop case, at phase $= 170°$ (maximum blowing phase of the cycle) for oscillatory control; $Re = 0.936$ million, $F^+ = 0.46$, $\langle c_\mu \rangle = 0.11$%, medium grid.
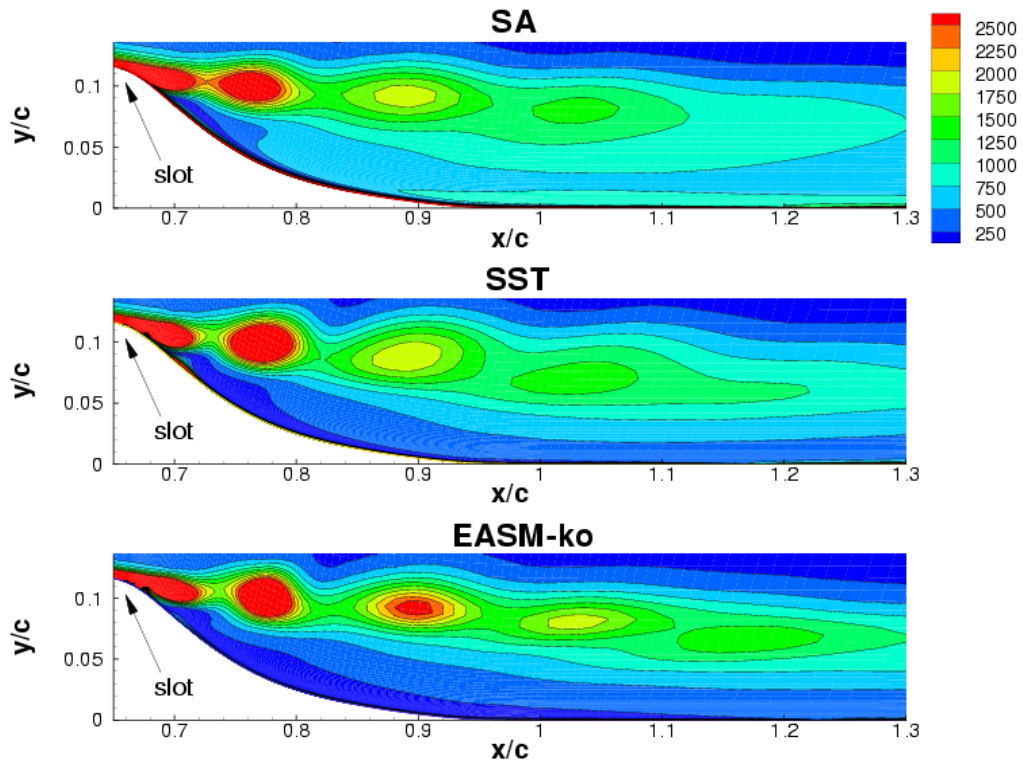
Figure 36. Vorticity contours (in 1/s) for lower F^+ than workshop case, at phase = $260°$ (cycle changing from blowing to suction) for oscillatory control; $Re = 0.936$ million, $F^+ = 0.46$, $\langle c_\mu \rangle = 0.11$%, medium grid.
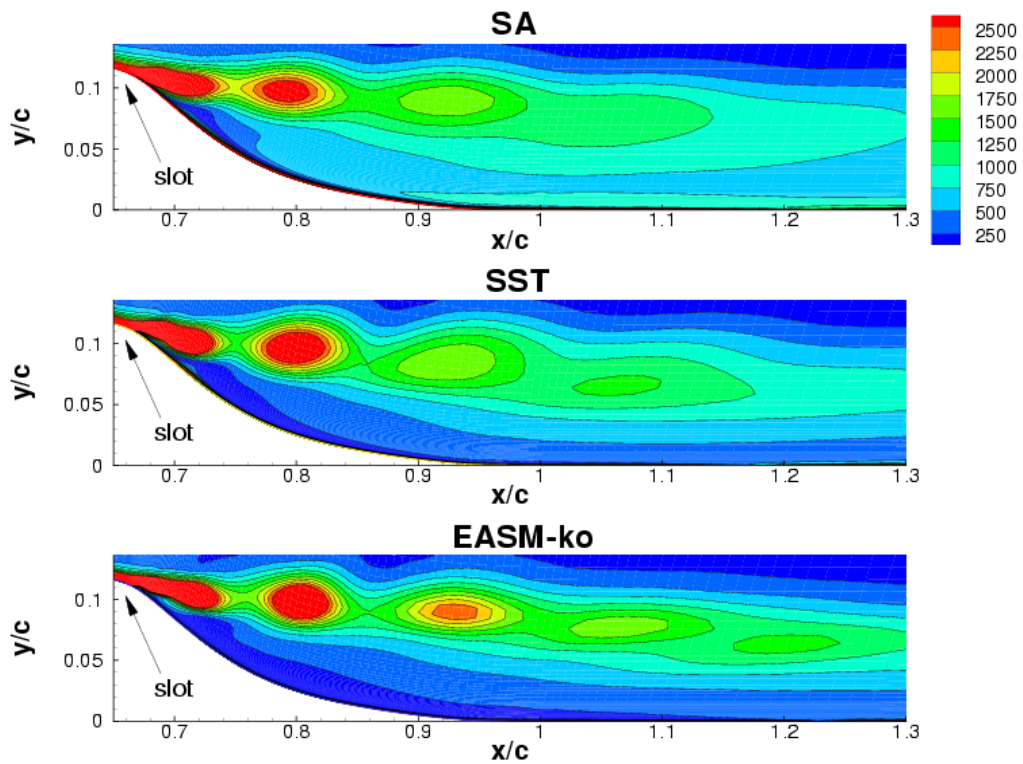

Figure 37. Vorticity contours (in 1/s) for lower F^+ than workshop case, at phase = $350°$ (maximum suction phase of the cycle) for oscillatory control; $Re = 0.936$ million, $F^+ = 0.46$, $\langle c_\mu \rangle = 0.11$%, medium grid.

Figure 38. Vorticity contours (in 1/s) for higher F^+ than workshop case, at phase = $80°$ (cycle changing from suction to blowing) for oscillatory control; $Re = 0.936$ **million,** $F^+ = 2.00$, $\langle c_\mu \rangle = 0.11$**%, medium grid.**

Figure 39. Vorticity contours (in 1/s) for higher F^+ than workshop case, at phase = $170°$ (maximum blowing phase of the cycle) for oscillatory control; $Re = 0.936$ **million,** $F^+ = 2.00$, $\langle c_\mu \rangle = 0.11$**%, medium grid.**

Figure 40. Vorticity contours (in 1/s) for higher F^+ than workshop case, at phase = $260°$ (cycle changing from blowing to suction) for oscillatory control; $Re = 0.936$ million, $F^+ = 2.00$, $\langle c_\mu \rangle = 0.11$%, medium grid.

Figure 41. Vorticity contours (in 1/s) for higher F^+ than workshop case, at phase = $350°$ (maximum suction phase of the cycle) for oscillatory control; $Re = 0.936$ million, $F^+ = 2.00$, $\langle c_\mu \rangle = 0.11$%, medium grid.
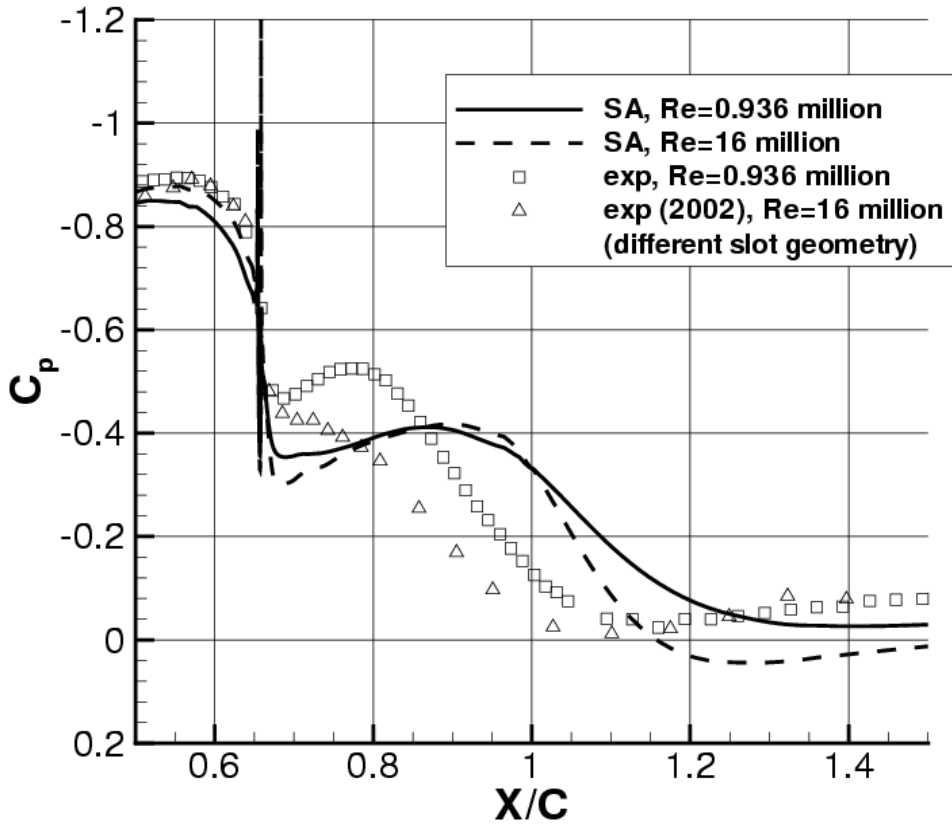
Figure 42. Effect of Reynolds number on long-time-averaged surface pressure coefficients for oscillatory control; $F^+ = 0.77$, $\langle c_\mu \rangle = 0.11$**%, SA model on medium grid.**
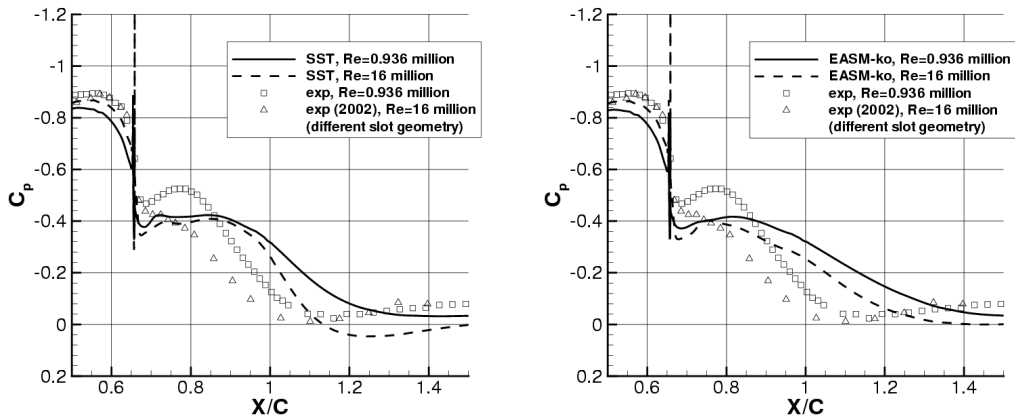
Figure 43. Effect of Reynolds number on long-time-averaged surface pressure coefficients for oscillatory control; $F^+ = 0.77$, $\langle c_\mu \rangle = 0.11$**%, SST (left) and EASM-ko (right) models on medium grid.**
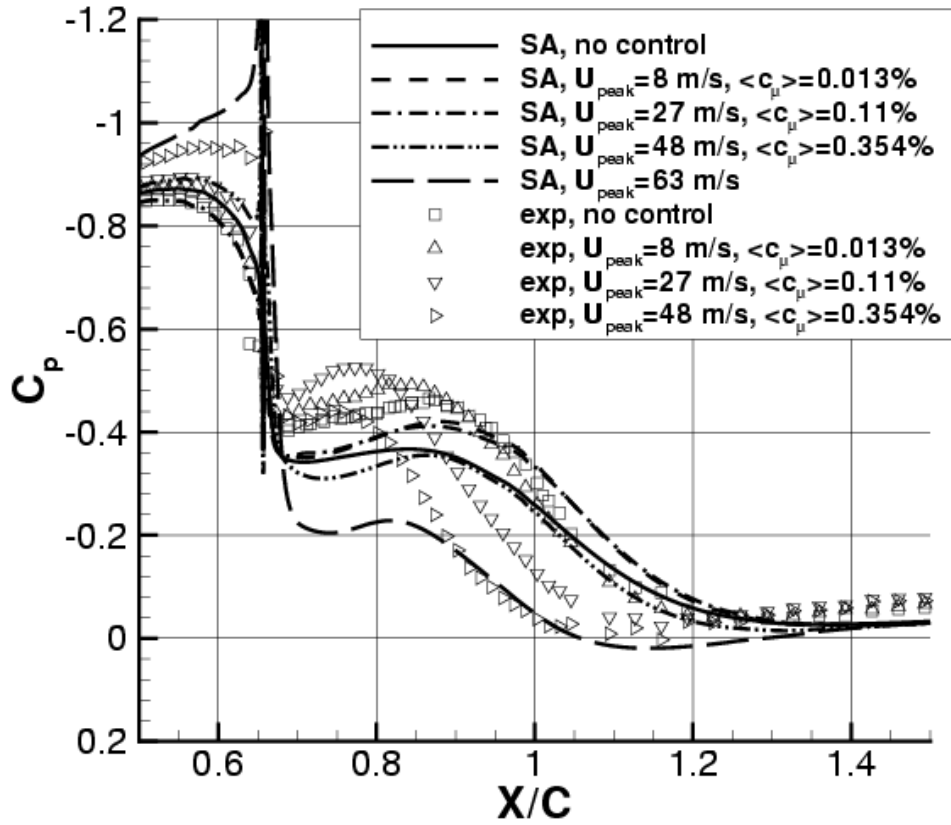
Figure 44. Effect of $\langle c_\mu \rangle$ on long-time-averaged surface pressure coefficients for oscillatory control; $Re = 0.936$ million, $F^+ = 0.77$, SA model on medium grid.
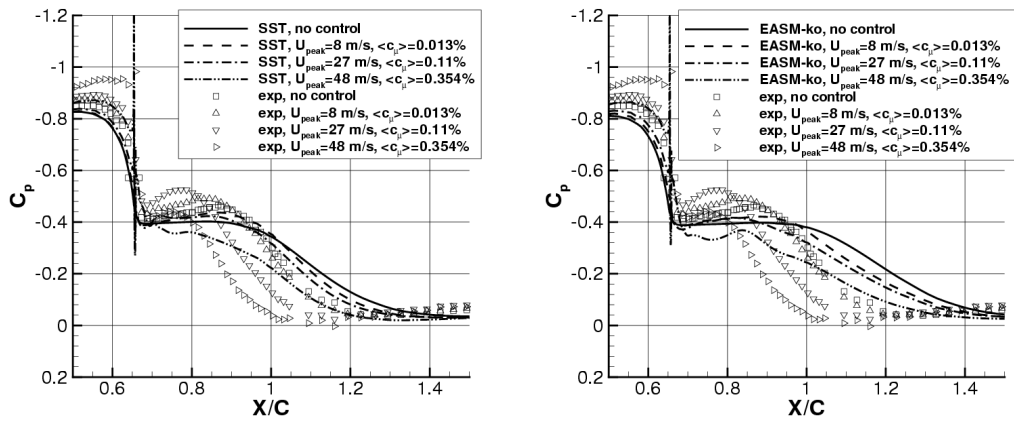
Figure 45. Effect of $\langle c_\mu \rangle$ on long-time-averaged surface pressure coefficients for oscillatory control; $Re = 0.936$ million, $F^+ = 0.77$, SST (left) and EASM-ko (right) models on medium grid.
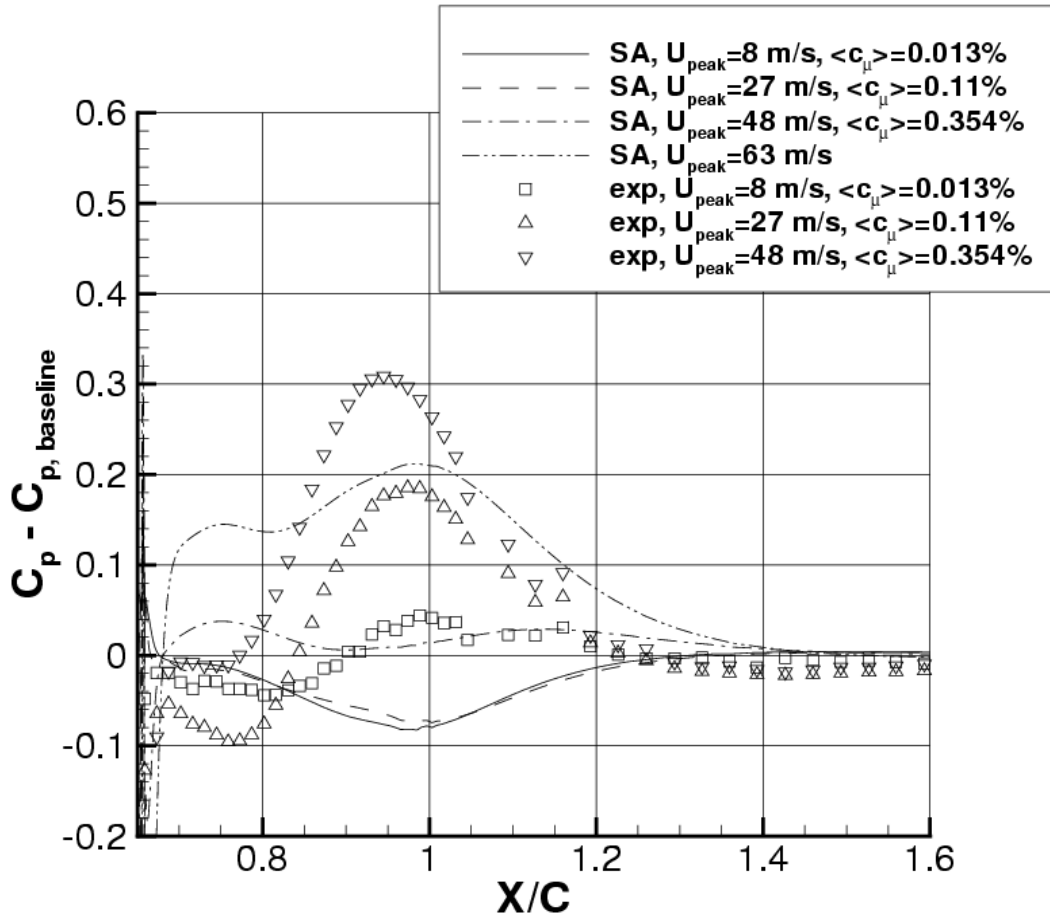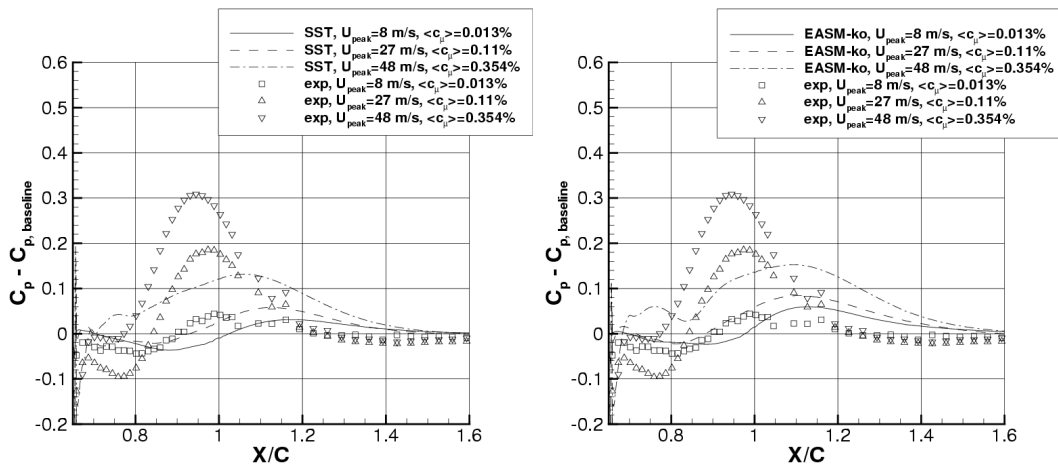
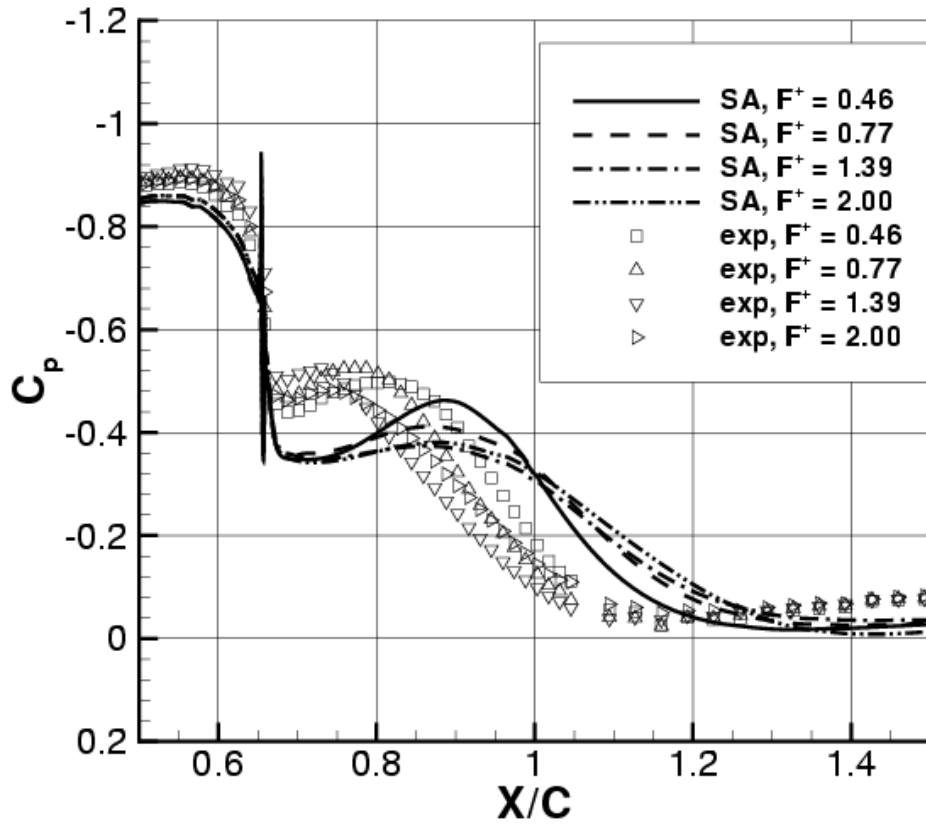**Figure 46. Effect of $\langle c_\mu \rangle$ on long-time-averaged surface pressure coefficients for oscillatory control relative to baseline (no control);** $Re = 0.936$ **million,** $F^+ = 0.77$**, SA model on medium grid.**

Figure 47. Effect of $\langle c_\mu \rangle$ on long-time-averaged surface pressure coefficients for oscillatory control relative to baseline (no control); $Re = 0.936$ **million,** $F^+ = 0.77$**, SST (left) and EASM-ko (right) models on medium grid.**
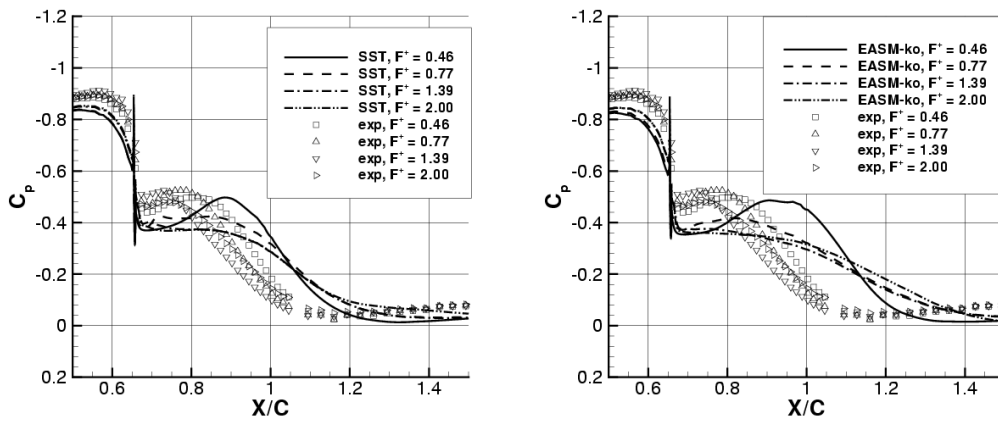
Figure 48. Effect of F^+ on long-time-averaged surface pressure coefficients for oscillatory control; $Re = 0.936$ **million,** $\langle c_\mu \rangle = 0.11$**%, SA model on medium grid.**

Figure 49. Effect of F^+ on long-time-averaged surface pressure coefficients for oscillatory control; $Re = 0.936$ **million,** $\langle c_\mu \rangle = 0.11$**%, SST (left) and EASM-ko (right) models on medium grid.**
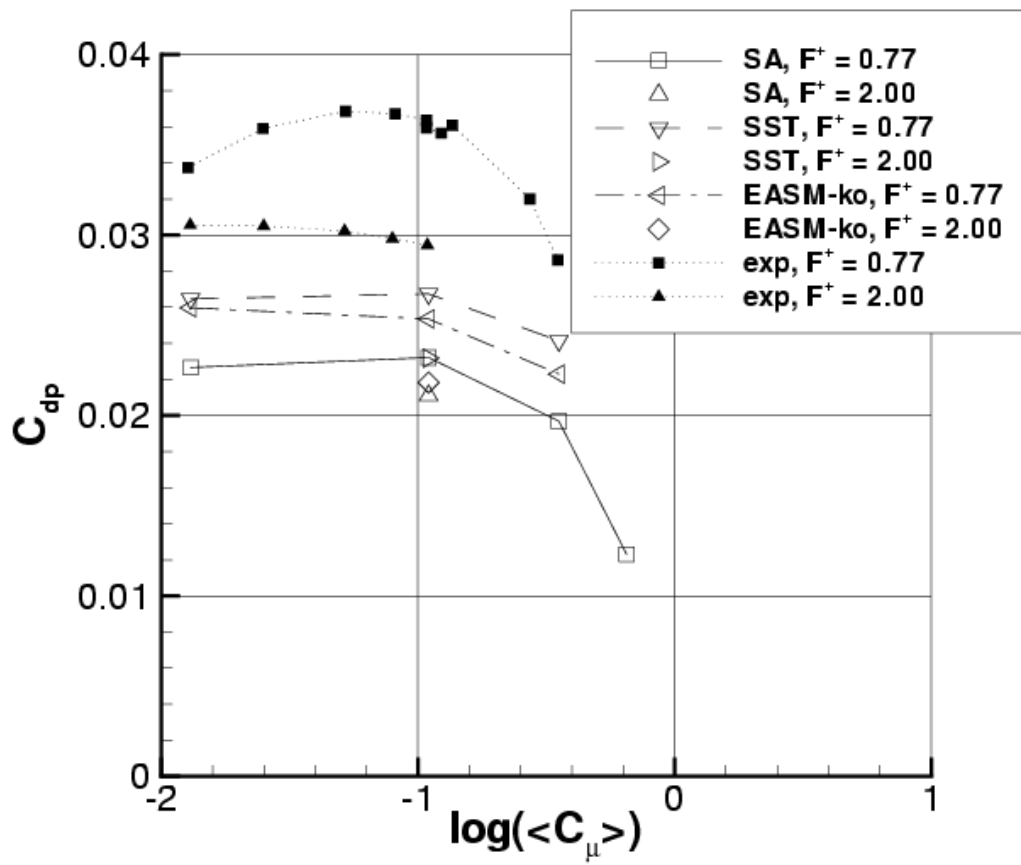
Figure 50. Pressure drag coefficient as a function of $\langle c_\mu \rangle$ for oscillatory control; $Re = 0.936$ million, medium grid.
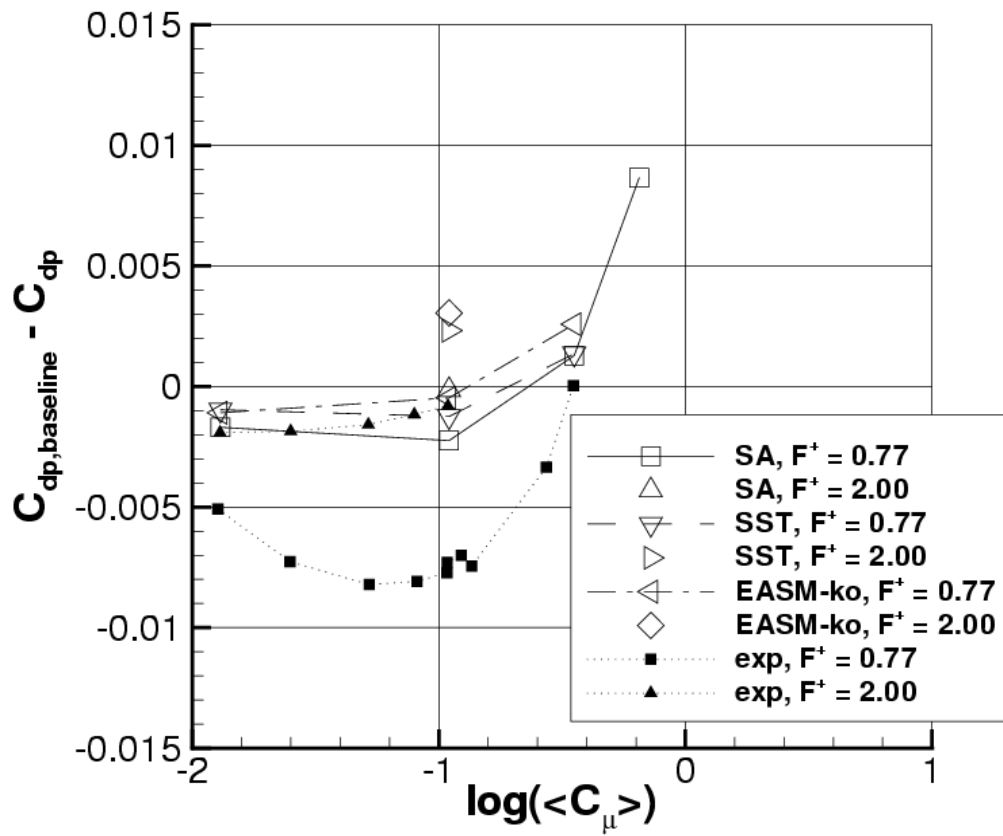
Figure 51. Pressure drag coefficient relative to baseline (no control) as a function of $\langle c_\mu \rangle$ for oscillatory control; $Re = 0.936$ million, medium grid.

REPORT DOCUMENTATION PAGE

Form Approved
OMB No. 0704-0188

1. REPORT DATE *(DD-MM-YYYY)*	2. REPORT TYPE	3. DATES COVERED *(From - To)*
01-09-2007	Technical Memorandum	

4. TITLE AND SUBTITLE

Parametric Study of Flow Control Over a Hump Model Using and Unsteady Reynolds-Averaged Navier-Stokes Code

5a. CONTRACT NUMBER

5b. GRANT NUMBER

5c. PROGRAM ELEMENT NUMBER

6. AUTHOR(S)

Rumsey, Christopher L.; and Greenblatt, David

5d. PROJECT NUMBER

5e. TASK NUMBER

5f. WORK UNIT NUMBER

561581.02.08

7. PERFORMING ORGANIZATION NAME(S) AND ADDRESS(ES)

NASA Langley Research Center
Hampton, VA 23681-2199

8. PERFORMING ORGANIZATION REPORT NUMBER

L-19386

9. SPONSORING/MONITORING AGENCY NAME(S) AND ADDRESS(ES)

National Aeronautics and Space Administration
Washington, DC 20546-0001

10. SPONSOR/MONITOR'S ACRONYM(S)

NASA

11. SPONSOR/MONITOR'S REPORT NUMBER(S)

NASA/TM-2007-214897

12. DISTRIBUTION/AVAILABILITY STATEMENT

Unclassified - Unlimited
Subject Category 01
Availability: NASA CASI (301) 621-0390

13. SUPPLEMENTARY NOTES

Rumsey: Langley Research Center, Hampton, Virginia; Greenblatt: Berlin University of Technology, Berlin, Germany
An electronic version can be found at http://ntrs.nasa.gov

14. ABSTRACT

This is an expanded version of a limited-length paper that appeared at the 5th International Symposium on Turbulence and Shear Flow Phenomena by the same authors. A computational study was performed for steady and oscillatory flow control over a hump model with flow separation to assess how well the steady and unsteady Reynolds-averaged Navier-Stokes equations predict trends due to Reynolds number, control magnitude, and control frequency. As demonstrated in earlier studies, the hump model case is useful because it clearly demonstrates a failing in all known turbulence models: they under-predict the turbulent shear stress in the separated region and consequently reattachment occurs too far downstream. In spite of this known failing, three different turbulence models were employed to determine if trends can be captured even though absolute levels are not. Overall the three turbulence models showed very similar trends as experiment for steady suction, but only agreed qualitatively with some of the trends for oscillatory control.

15. SUBJECT TERMS

Flow control; Synthetic jet; Turbulence; Separation; Reattachment

16. SECURITY CLASSIFICATION OF:			17. LIMITATION OF ABSTRACT	18. NUMBER OF PAGES	19a. NAME OF RESPONSIBLE PERSON
a. REPORT	b. ABSTRACT	c. THIS PAGE			STI Help Desk (email: help@sti.nasa.gov)
U	U	U	UU	48	19b. TELEPHONE NUMBER *(Include area code)* (301) 621-0390

Standard Form 298 (Rev. 8-98)
Prescribed by ANSI Std. Z39.18